Systematic irradiation studies and Quality Assurance of silicon strip sensors for the CBM Silicon Tracking System

P. Larionov
✉ p.larionov@gsi.de

Laboratori nazionali di Frascati, September 2016

Outline

- CBM experiment
- Silicon Tracking System
- Double-sided silicon strip sensors
- Investigation on the radiation tolerance of the STS sensors
- Development of the Quality Assurance test stand for strip diagnostics
- Summary

The Compressed Baryonic Matter Experiment

- To be built as a part of Facility for Antiproton and Ion Research (FAIR) in GSI, Darmstadt, Germany;

- Fixed target experiment;

- Heavy ion beams will be provided by SIS100, and later, SIS300 synchrotrons;

- SIS100: up to 11 AGeV for heavy ions, up to 30 GeV for protons;
- SIS300: up to 45 AGeV for heavy ions, up to 90 GeV for protons.

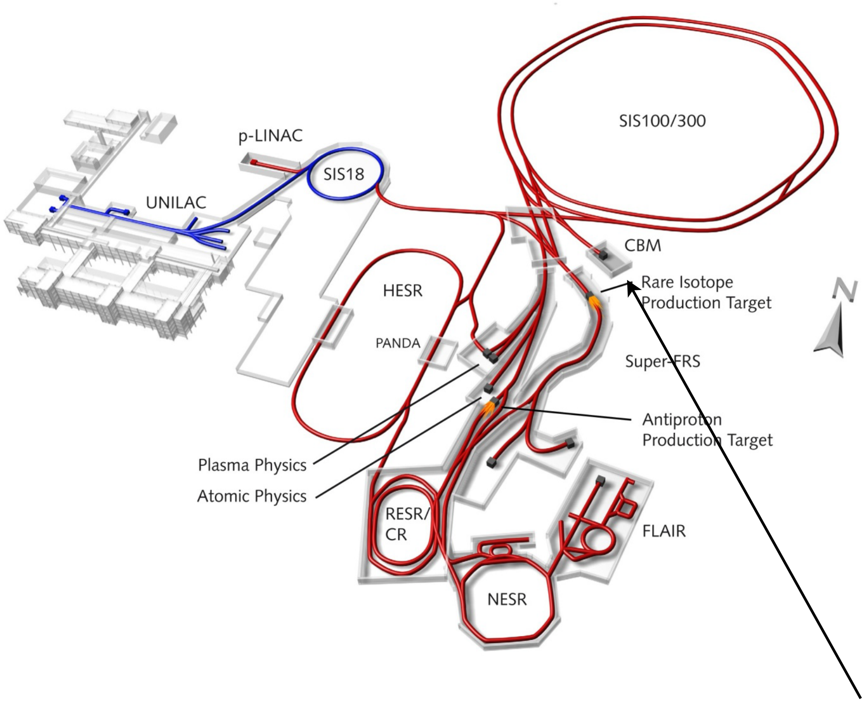

CBM cave

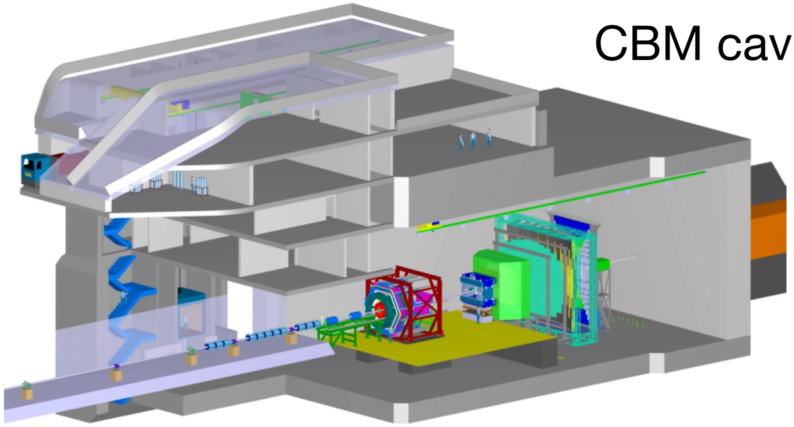

The Compressed Baryonic Matter Experiment

- Aim: study the QCD phase diagram in the region of high net-baryon densities and moderate temperatures;

- L-QCD not applicable in this region;

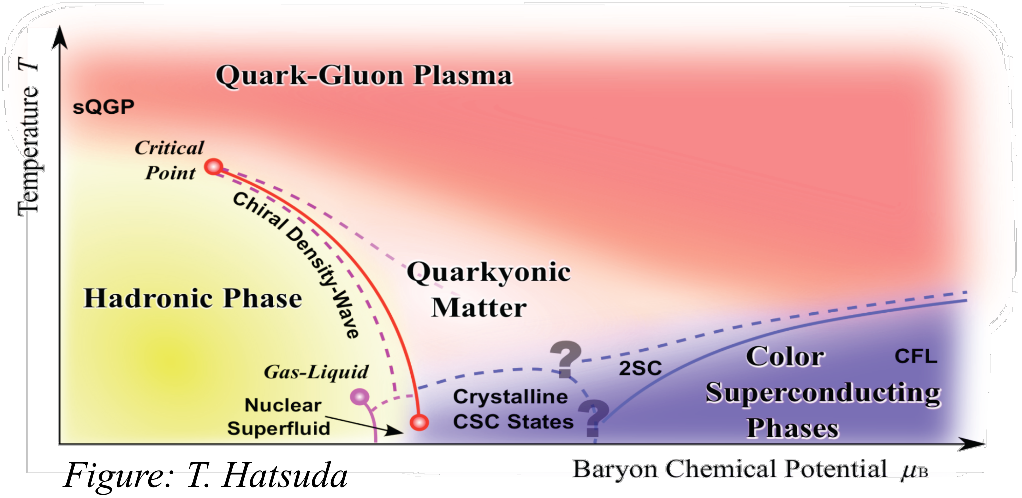

Figure: T. Hatsuda

The Compressed Baryonic Matter Experiment

- Aim: study the QCD phase diagram in the region of high net-baryon densities and moderate temperatures;

- L-QCD not applicable in this region;

- Already at SIS100 energies the fireball is compressed (> 8 ρ_0);

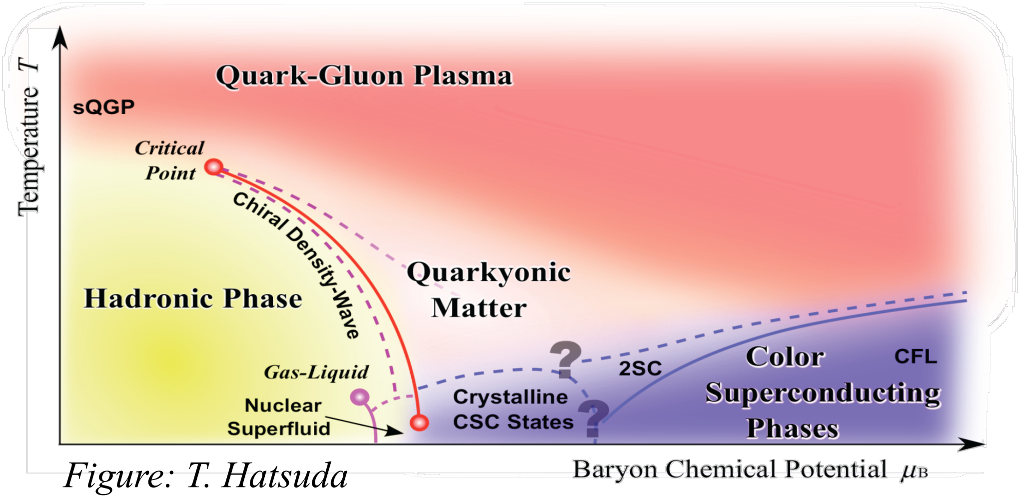

Figure: T. Hatsuda

Au+Au 10 A GeV

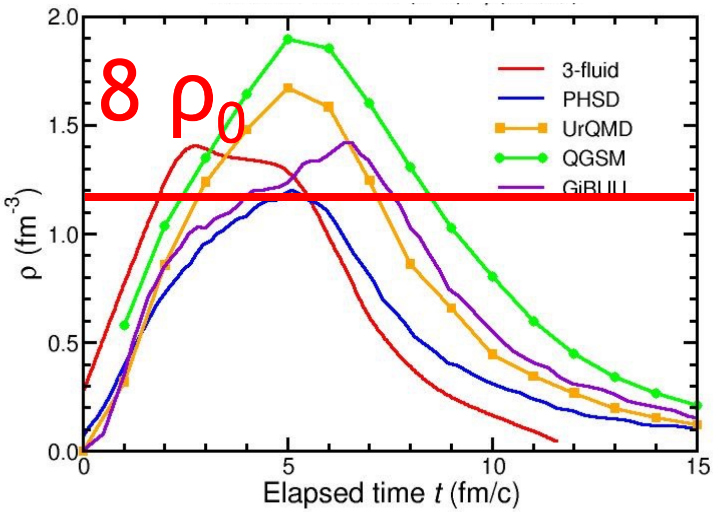

The Compressed Baryonic Matter Experiment

- Aim: study the QCD phase diagram in the region of high net-baryon densities and moderate temperatures;

- L-QCD not applicable in this region;

- Diagnostic probes sensitive to the dense phase of the fireball evolution: light vector mesons, multi-strange (anti-) hyperons, charmed particles → rarely produced;

- High intensity heavy-ion beams, up to 10^9 ions/s, interaction rates up to 10 MHz.

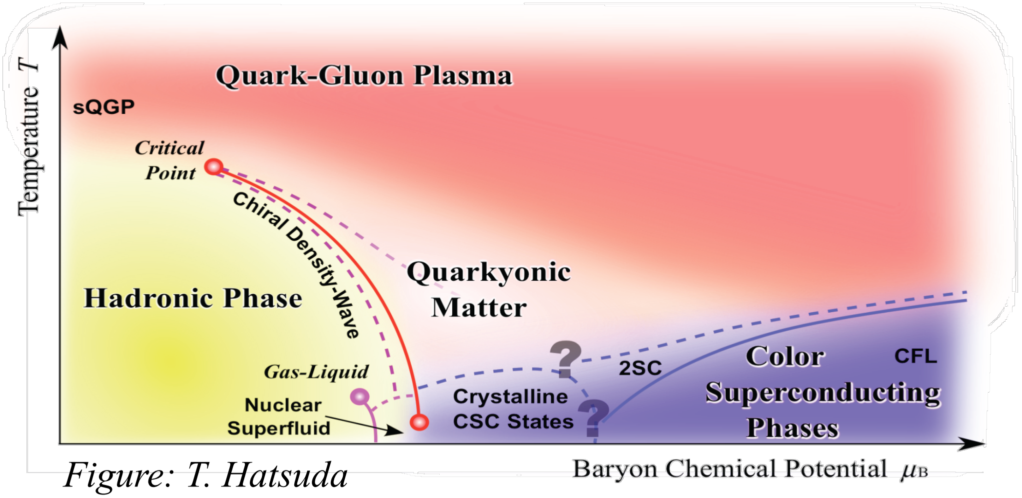

Figure: T. Hatsuda

Particle yields in central Au+Au 4 A GeV

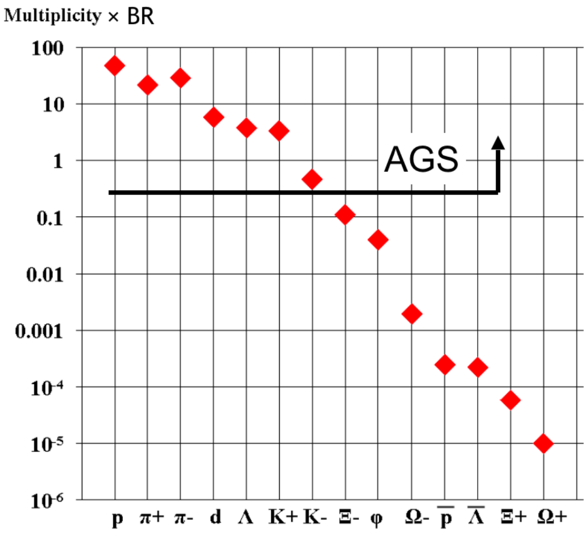

The Compressed Baryonic Matter Experiment

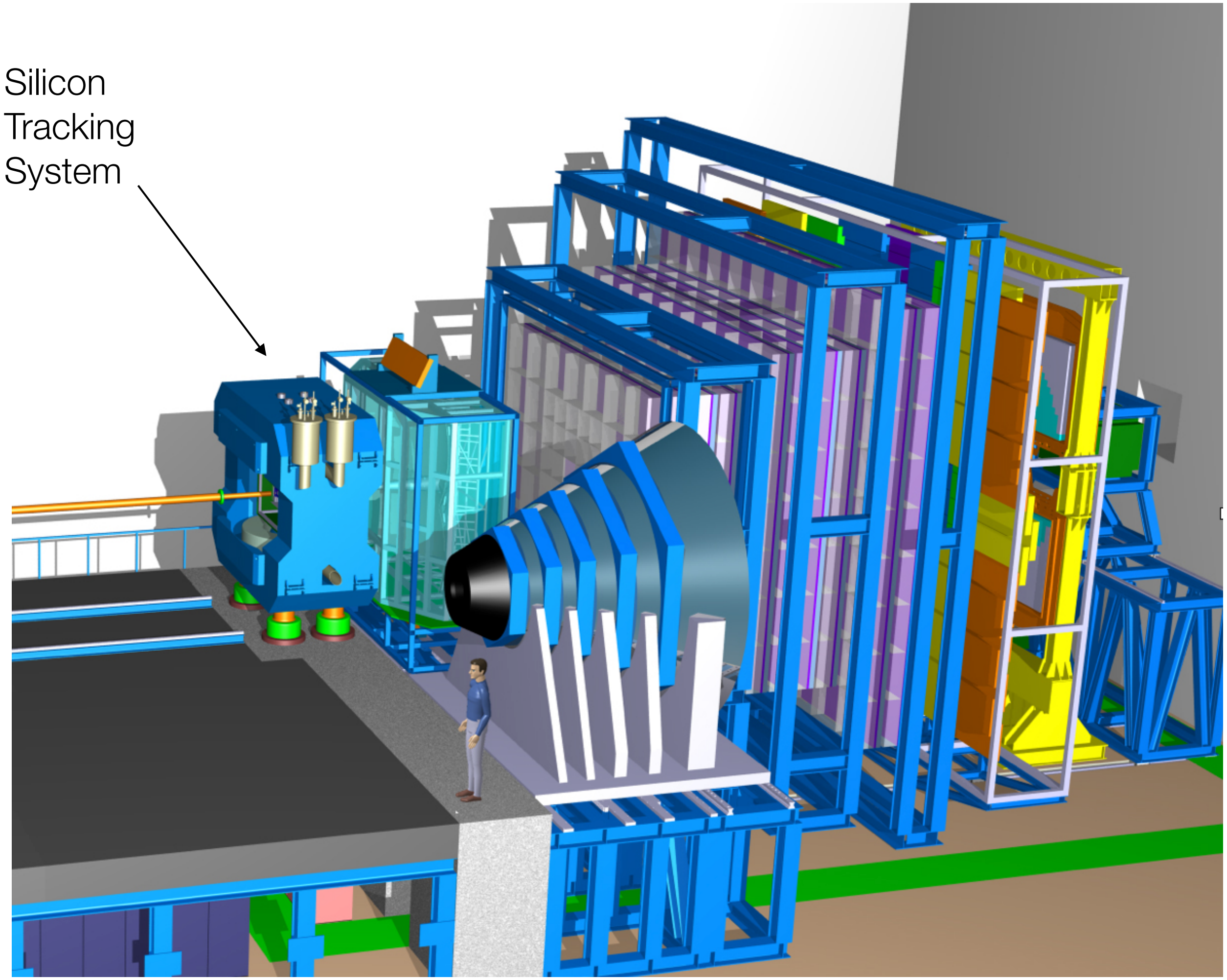

Detectors for particle identification. Electron+hadron (installed) and muon (parking position) setups.

The Silicon Tracking System

- Task: reconstruct the tracks of charged particles and determine their momenta;

- Track reconstruction efficiency > 95% (for *p* > 1 GeV/c), momentum resolution ~ 1.5%; single hit efficiency close to 100% at low material budget;

- Interaction rates up to 10 MHz;

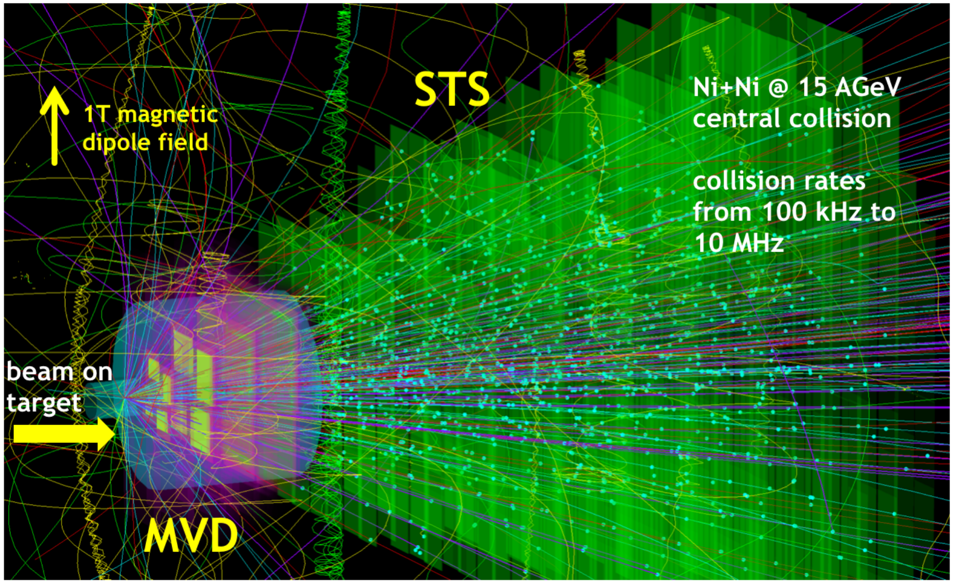

The Silicon Tracking System

- Task: reconstruct the tracks of charged particles and determine their momenta;
- Track reconstruction efficiency > 95% (for $p > 1$ GeV/c), momentum resolution ~ 1.5%; single hit efficiency close to 100% at low material budget;
- Interaction rates up to 10 MHz;
- Electronics outside of the physics aperture ($2.5^{\circ} < \Theta < 25^{\circ}$) for low material budget;
- 8 stations located downstream of the target inside the magnetic field.

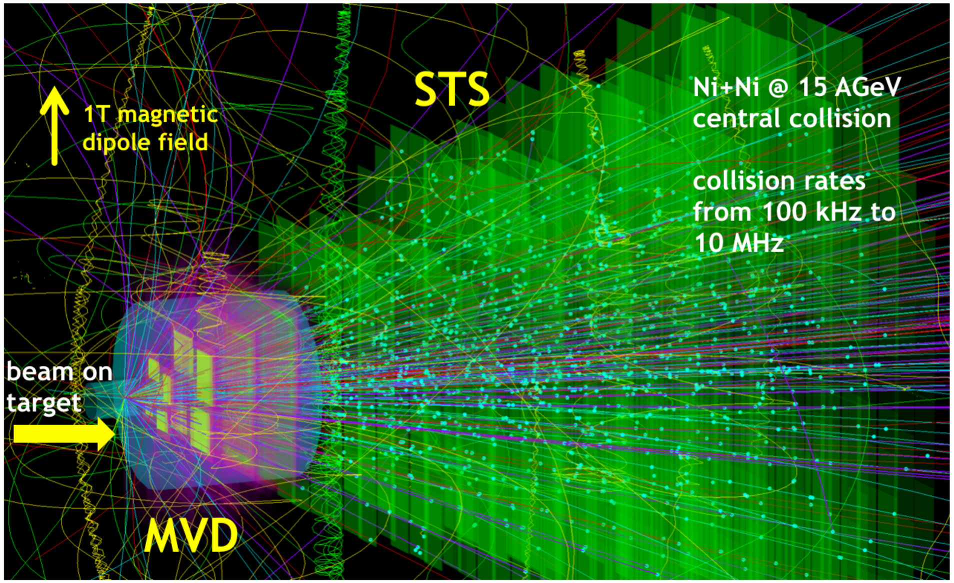

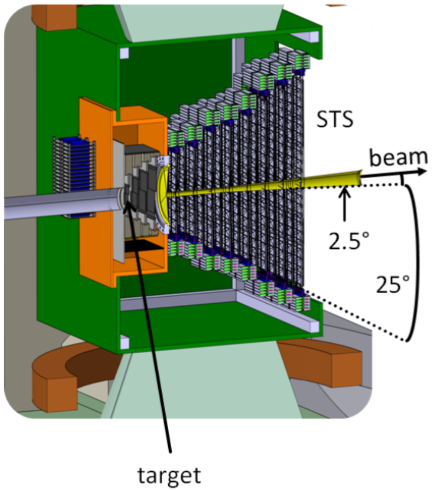

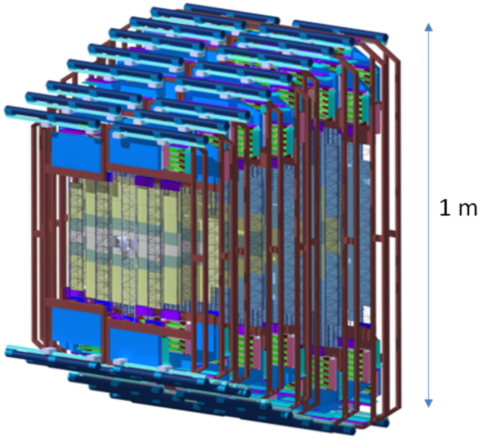

The Silicon Tracking System

- Task: reconstruct the tracks of charged particles and determine their momenta;
- Track reconstruction efficiency > 95% (for *p* > 1 GeV/c), momentum resolution ~ 1.5%; single hit efficiency close to 100% at low material budget;
- Interaction rates up to 10 MHz;
- Electronics outside of the physics aperture (2.5°< Θ < 25°) for low material budget;
- 8 stations located downstream of the target inside the magnetic field.

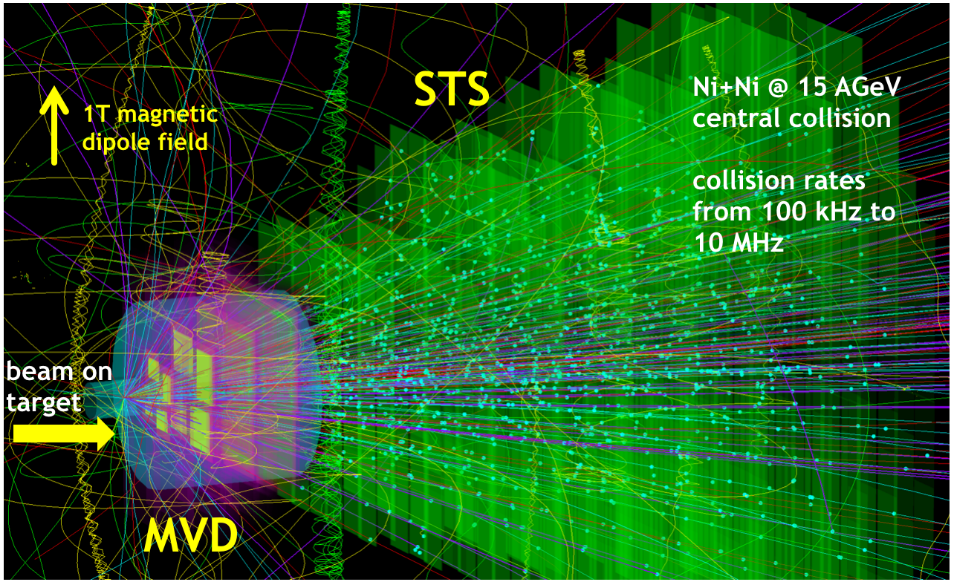

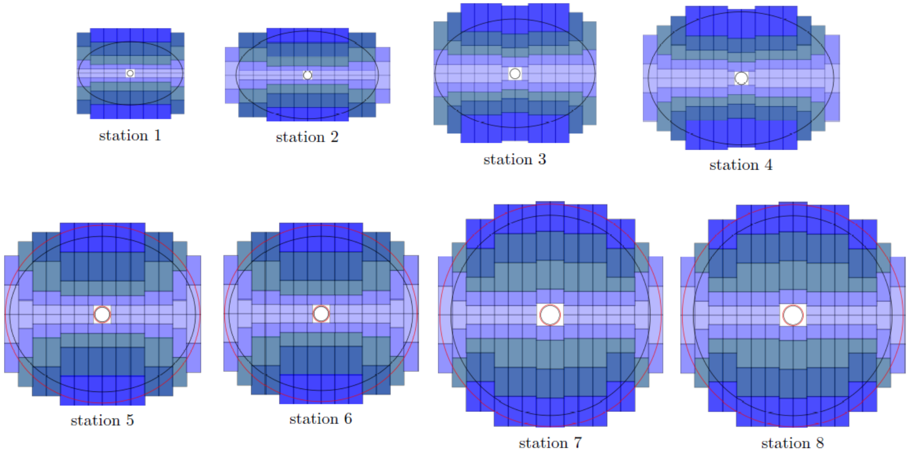

Station layout

The Silicon Tracking System

- Low material budget: < 0.3% - 1.18% X_0 in the inner areas;
- Double-sided silicon strip sensors;
- Module: sensor + r/o microcables + r/o electronics;
- Readout from one edge.

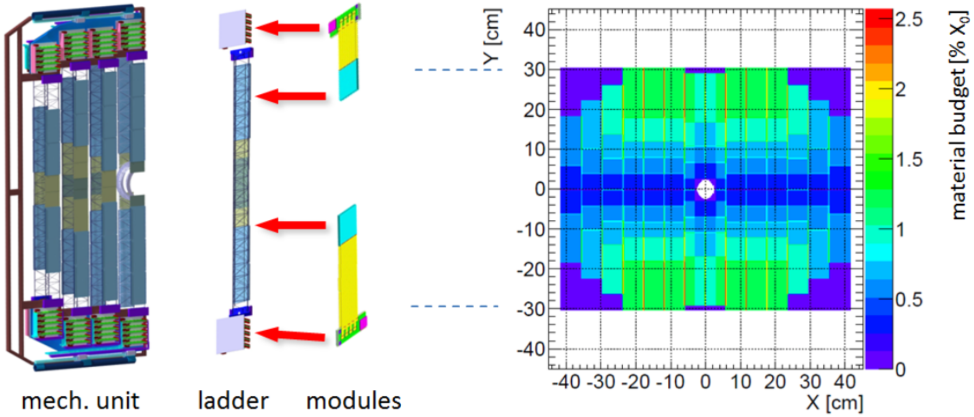

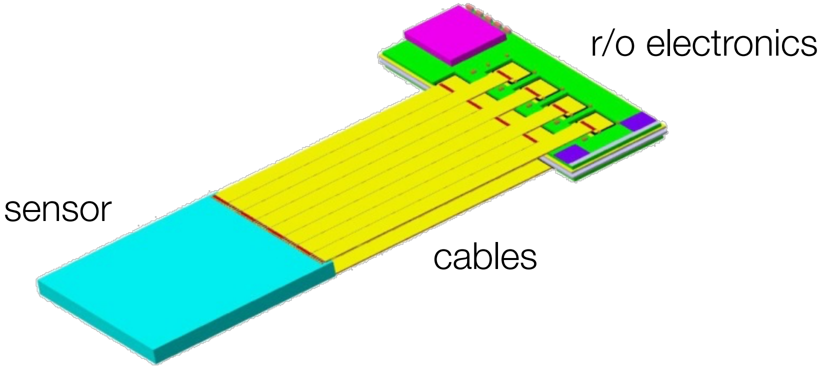

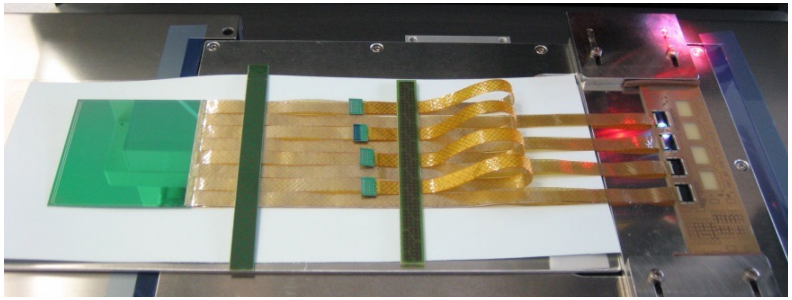

Double-sided strip sensors

- p^+-n^--n^+ silicon, double-sided;
- 1024 strips per side;
- Stereo angle front-back side 7.5°;
- 58 μm strip pitch, ~300 μm thick;
- Strip length: 2/4/6/12 cm;
- Poly-Si biasing structure;
- AC-coupled readout;
- Corner strips interconnection: additional metal layer (double metal) or external cable;
- Miniature (baby) sensors: orthogonal strips, 50 μm strip pitch, same wafer;
- Vendors: Hamamatsu (Japan), CiS (Germany).

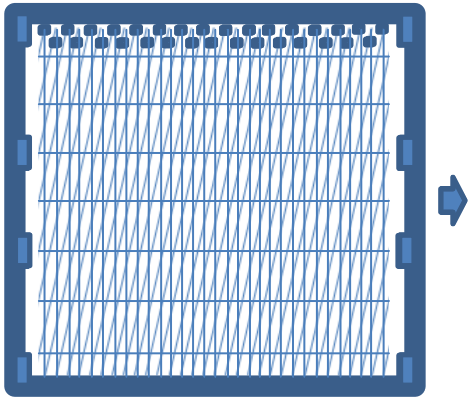

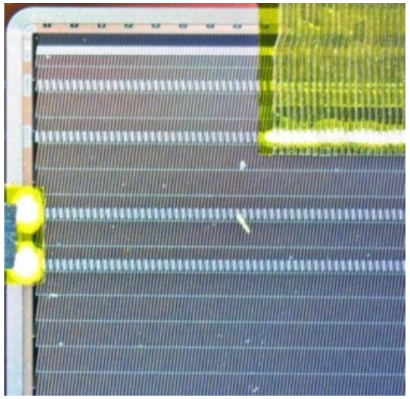

CBM prototype sensor corner view: readout cable attached

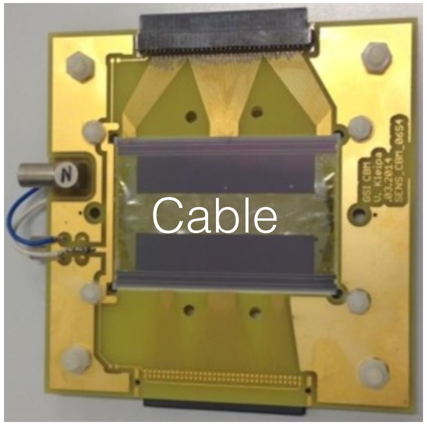

Prototype sensor with an external cable attached, clamped in the PCB

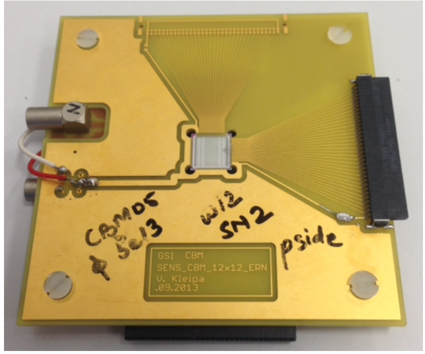

Miniature (or baby) sensor, clamped in the PCB

Double-sided strip sensors

- p^+-n^--n^+ silicon, double-sided;
- 1024 strips per side;
- Stereo angle front-back side 7.5°;
- 58 µm strip pitch, ~300 µm thick;
- Strip length: 2/4/6/12 cm;
- Poly-Si biasing structure;
- AC-coupled readout;
- Corner strips interconnection: additional metal layer (double metal) or external cable;
- Miniature (baby) sensors: orthogonal strips, 50 µm strip pitch, same wafer;
- Vendors: Hamamatsu (Japan), CiS (Germany);
- Wafer: prototype sensor, miniature sensors, test structures.

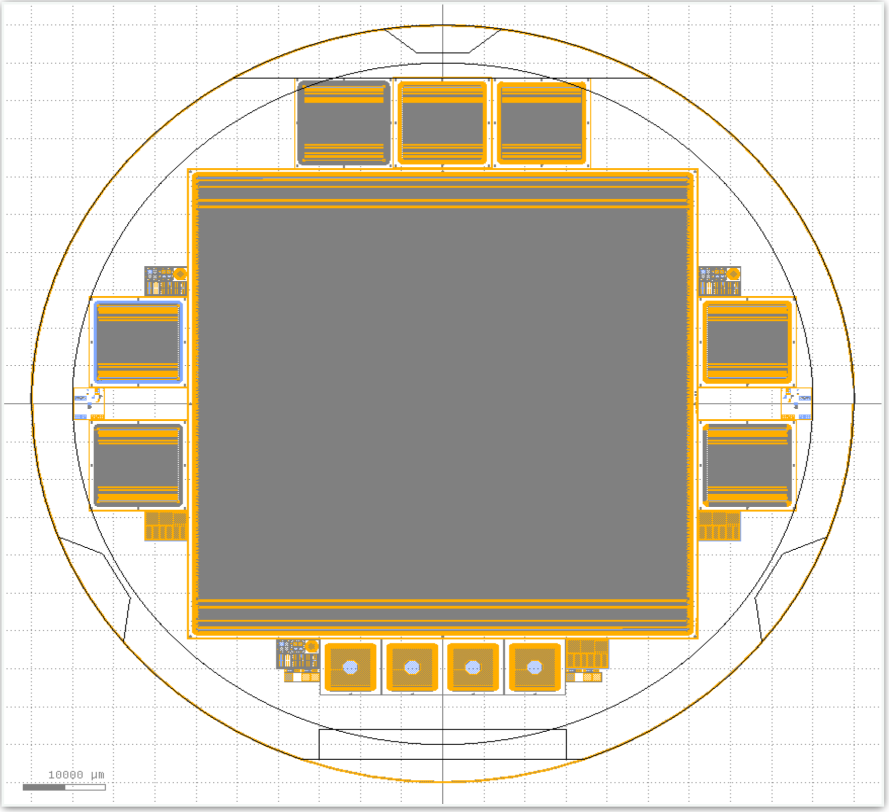

Schematic view of the wafer before dicing

Double-sided strip sensors

- p^+-n^--n^+ silicon, double-sided;
- 1024 strips per side;
- Stereo angle front-back side 7.5°;
- 58 μm strip pitch, ~300 μm thick;
- Strip length: 2/4/6/12 cm;
- Poly-Si biasing structure;
- AC-coupled readout;
- Corner strips interconnection: additional metal layer (double metal) or external cable;
- Miniature (baby) sensors: orthogonal strips, 50 μm strip pitch, same wafer;
- Wafer: prototype sensor, miniature sensors, test structures.

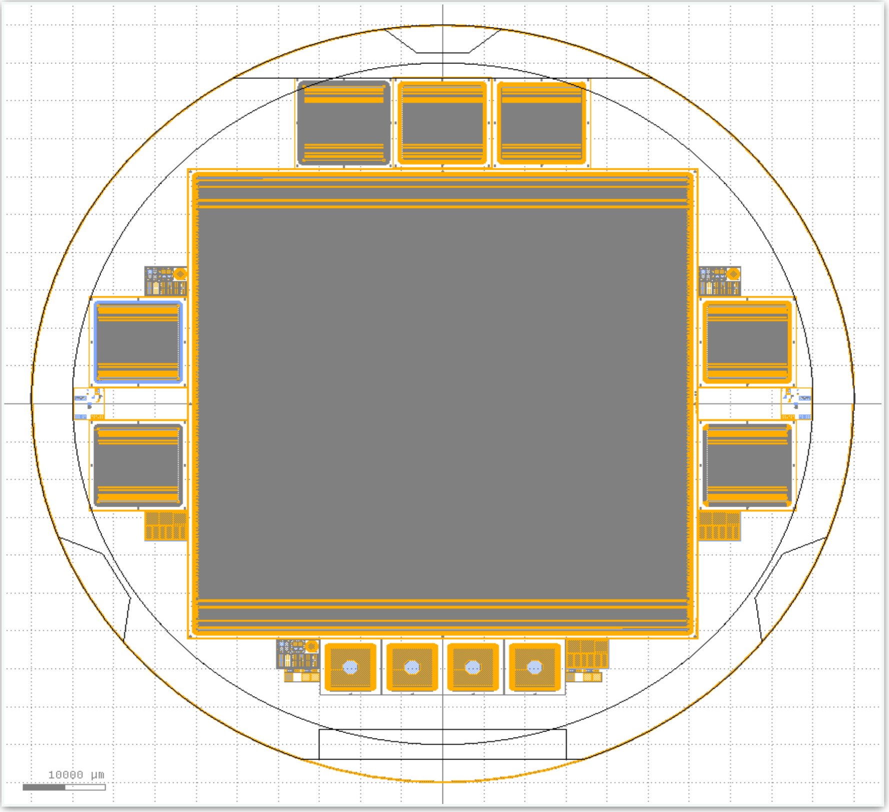

Schematic view of the wafer before dicing

Limitations of the sensors' performance: radiation damage, quality of the sensors

Investigation on the radiation tolerance of the STS sensors

NIEL for STS: FLUKA calculation

» Flux: neutrons, protons, pions, electrons, other;

» Lifetime fluence: 10^{14} cm^{-2} in 1 MeV neutron equivalent.

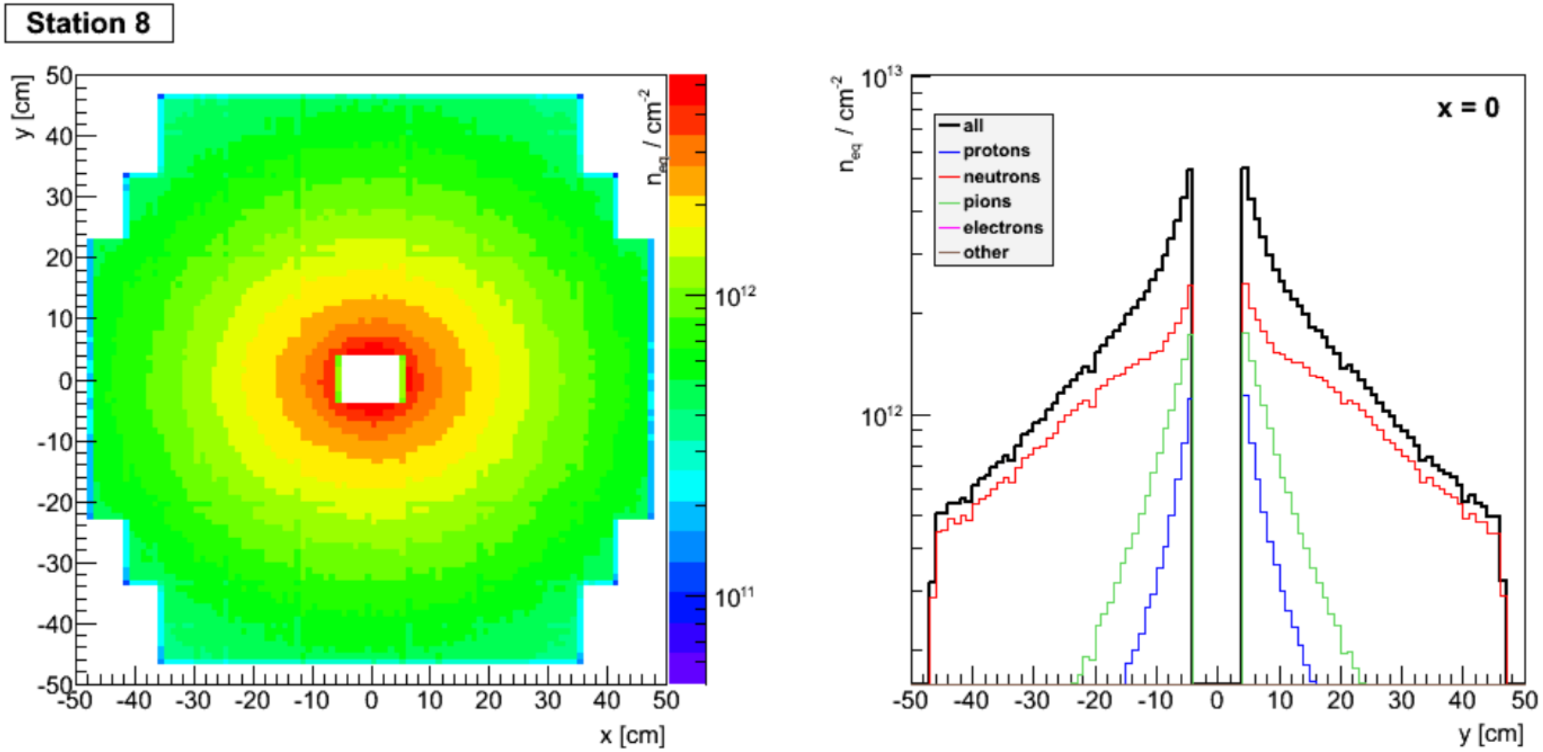

Accumulated NIEL: 25 AGeV Au+Au.

Irradiations

- **Neutron irradiation:** reactor neutrons at JSI, Ljubljana, Slovenia;
- Miniature sensors (2 batches), ~ 20 sensors;
- Fluences: from 1×10^{13} n_{eq}/cm^2 to 2×10^{14} n_{eq}/cm^2;

Reactor facility at JSI; Irradiation tube pointed

Irradiations

- **Neutron irradiation:** reactor neutrons at JSI, Ljubljana, Slovenia;
- Miniature sensors (2 batches), ~ 20 sensors;
- Fluences: from 1×10^{13} n_{eq}/cm^2 to 2×10^{14} n_{eq}/cm^2;

Reactor facility at JSI; Irradiation tube pointed

- **Proton irradiation:** 23 MeV protons at KIT, Karlsruhe, Germany;
- Prototype sensors;
- Fluence: 2×10^{14} n_{eq}/cm^2.

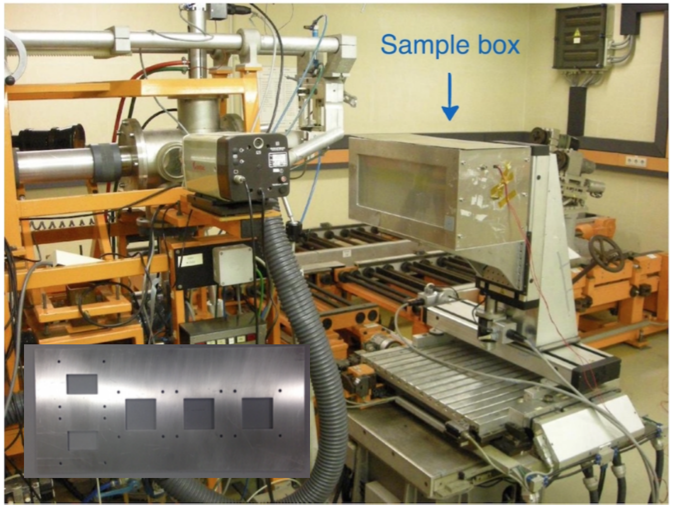

Irradiation facility at KIT

Leakage current as a function of the fluence

Measurements with n-irradiated **miniature sensors (CBM05)**:

» confirmed increase proportional to Φ;

» $\alpha = (5.52 \pm 0.05) \times 10^{-17}$ A/cm;

» → estimation of the I_{leak} at various levels of irradiation;

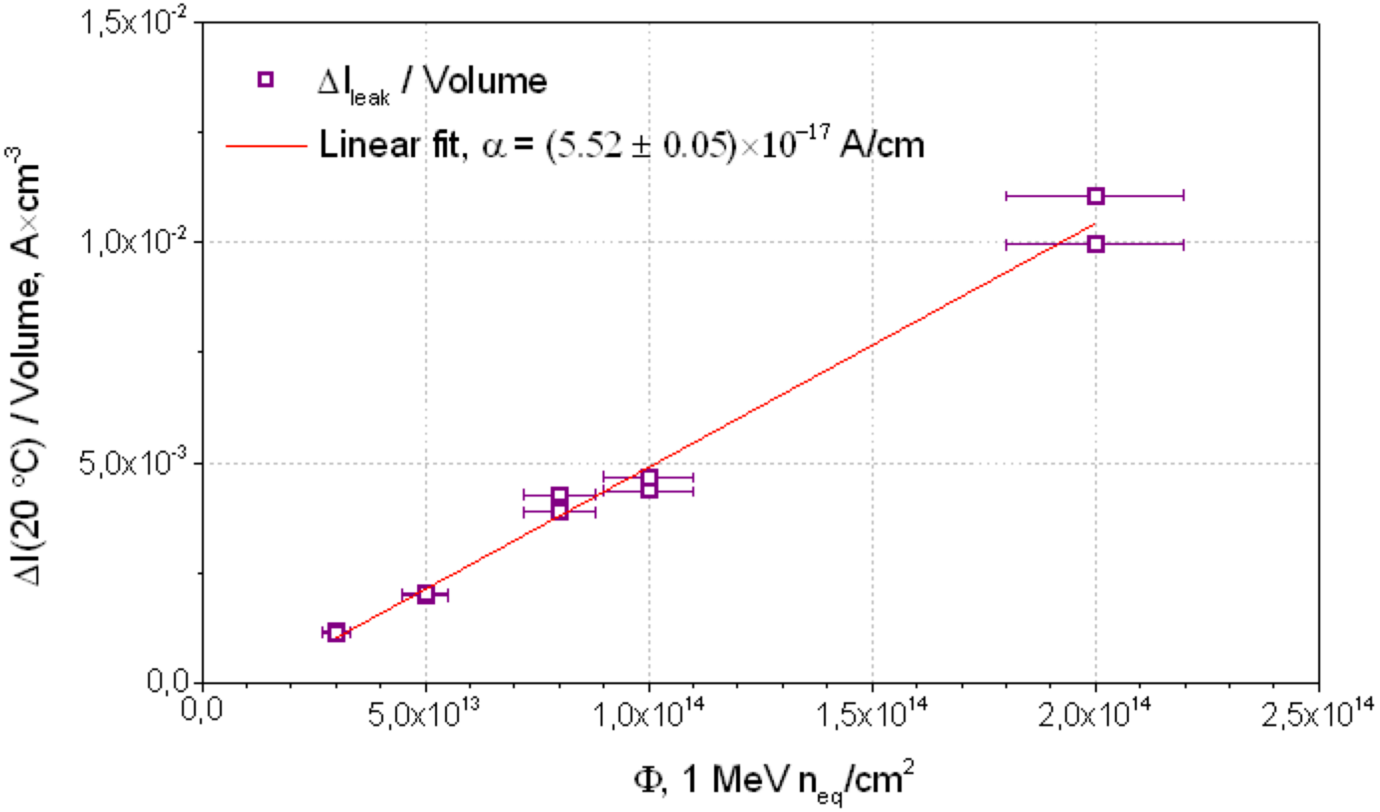

Leakage current as a function of the fluence

Measurements with **prototype sensors (CBM05, 06)** irradiated with protons:

» increases > 1 mA;

» using *α* extracted previously → I_{leak} (6×6 cm^2 sensor) ~ 1.15 mA (± 20 %);
I_{leak} (6×4 cm^2 sensor) ~ 0,85 mA (± 20 %);

» high leakage current → long-term stability.

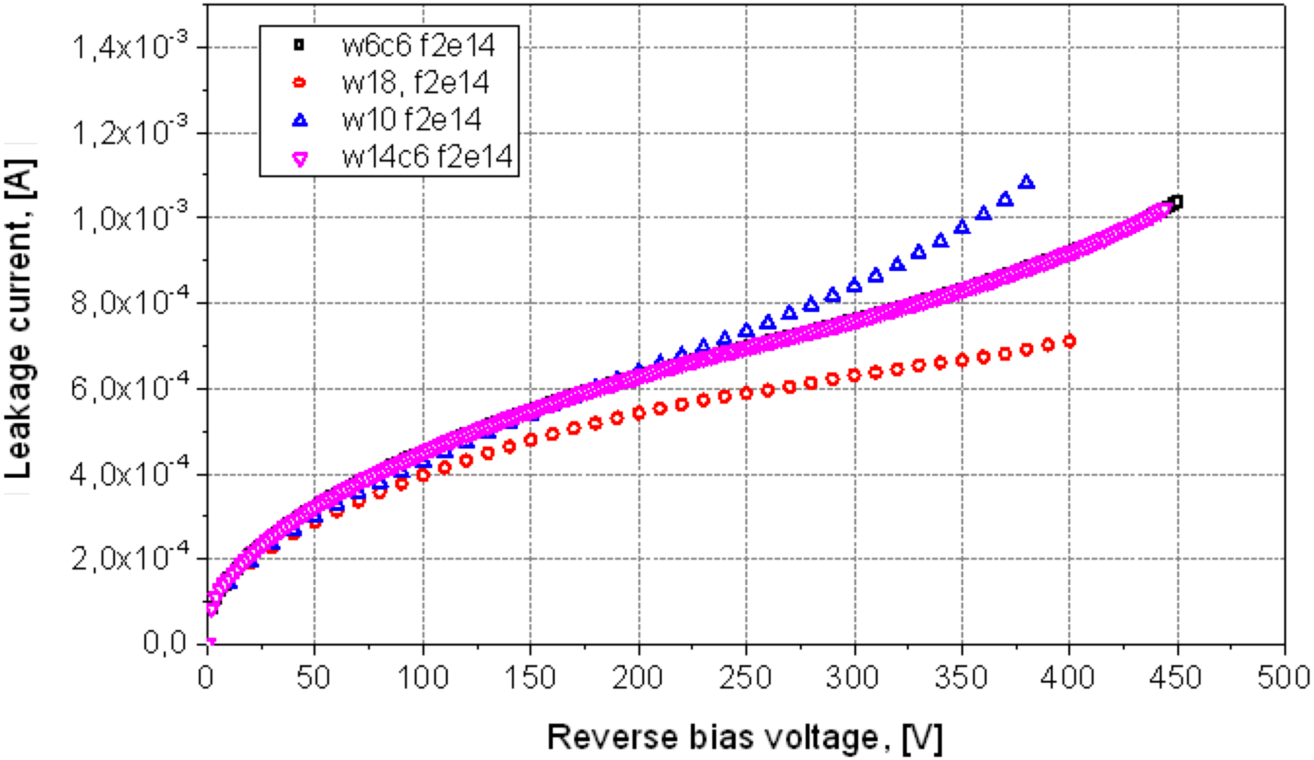

Evolution of the full depletion voltage

Measurements with n-irradiated **miniature sensors (CBM05)**, two batches:

» Experimental data + Hamburg model: calculation of $N_C + N_A(t_a = 6\ \mathrm{hrs})$, 290 µm sensor, $N_{eff,0} \approx 1.33 \times 10^{12}\ \mathrm{cm}^{-3}$ ($V_{fd,0} = 85$ V);

» Space charge sign inversion at $\approx 2.2 \times 10^{13}\ \mathrm{n_{eq}\ cm^{-2}}$.

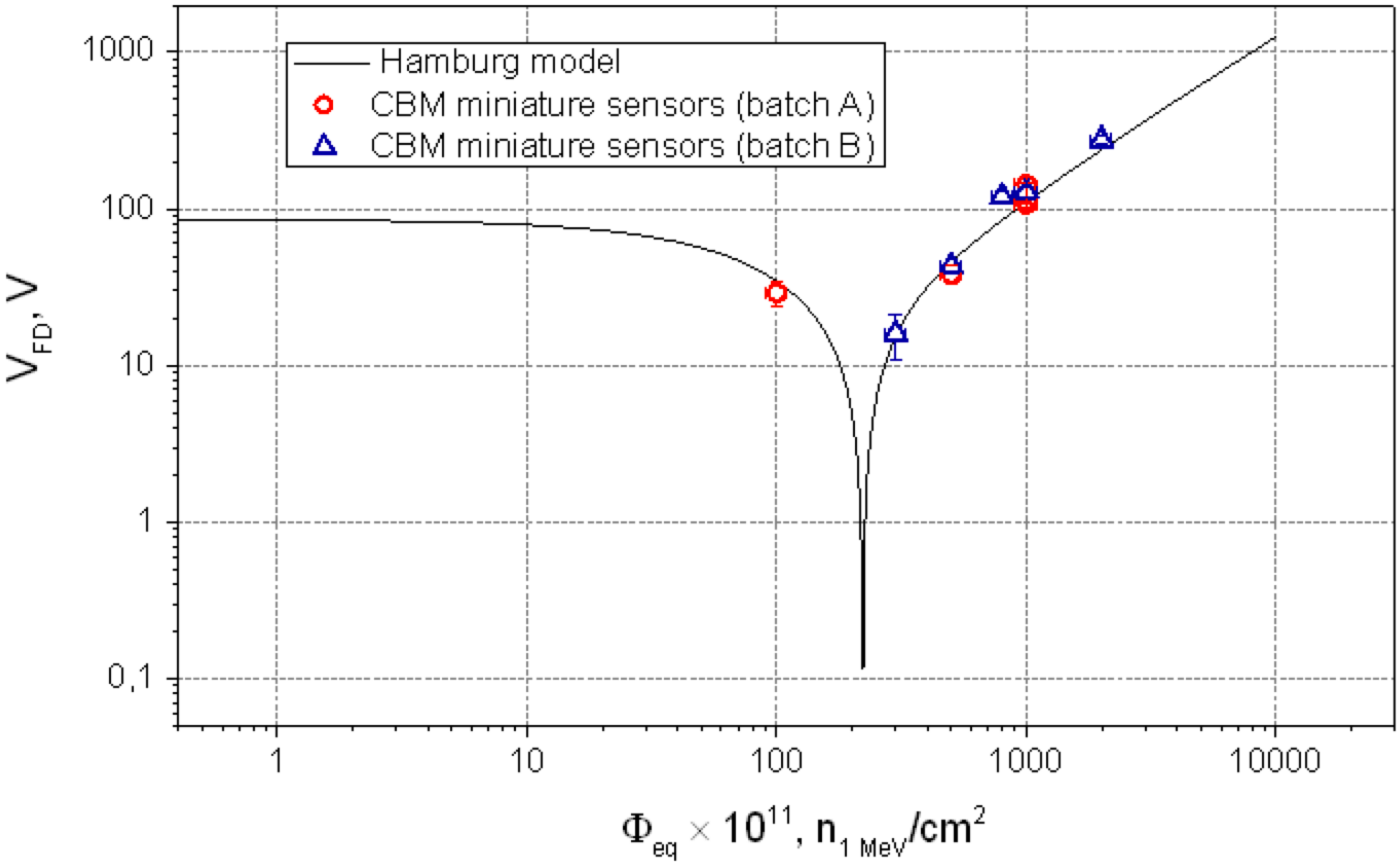

Evolution of charge collection

Measurements on n-irr. **miniature sensors**:

- » High voltages for high charge collection;
- » Considering V_{fd} extracted from C-V measurement: more than 200 V over depletion is needed in most of the cases;

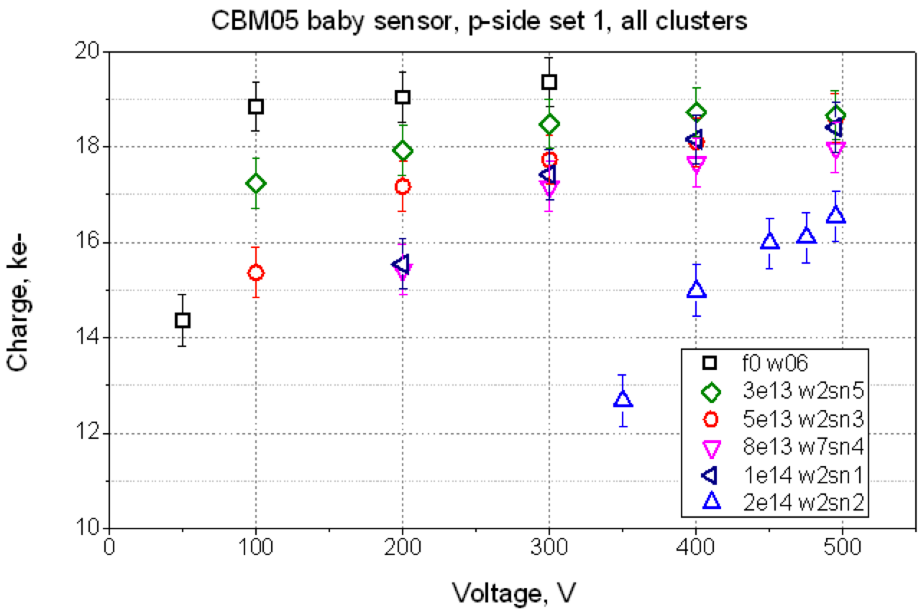

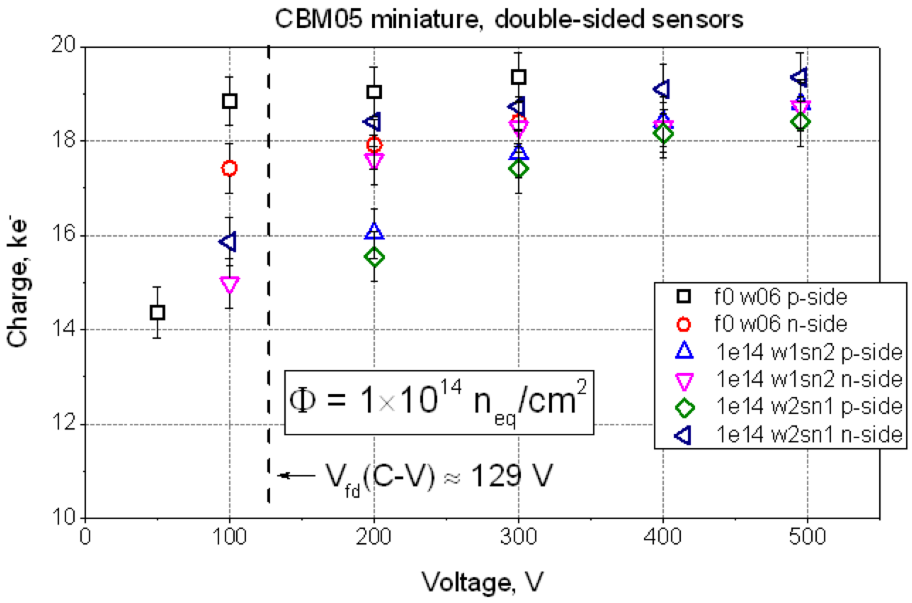

Evolution of charge collection

Measurements on n-irr. **miniature sensors**:

» High voltages for high charge collection;

» Considering V_{fd} extracted from C-V measurement: more than 200 V over depletion is needed in most of the cases;

» up to 1×10^{14} n_{eq} cm^{-2}:
$\approx$ 95% at *n*-side, $\approx$ 90% at *p*-side;

» beyond 1×10^{14} n_{eq} cm^{-2}:
p-side signal suppression;

» after the SCSI: junction at *n*-side, electric field non-uniform ($\Phi \geq 1\times10^{14}$ n_{eq} cm^{-2}), higher hole trapping probability, multiplication at highest field (*n*-side);

» Different charge collection before irradiation: thresholds, isolation structures.

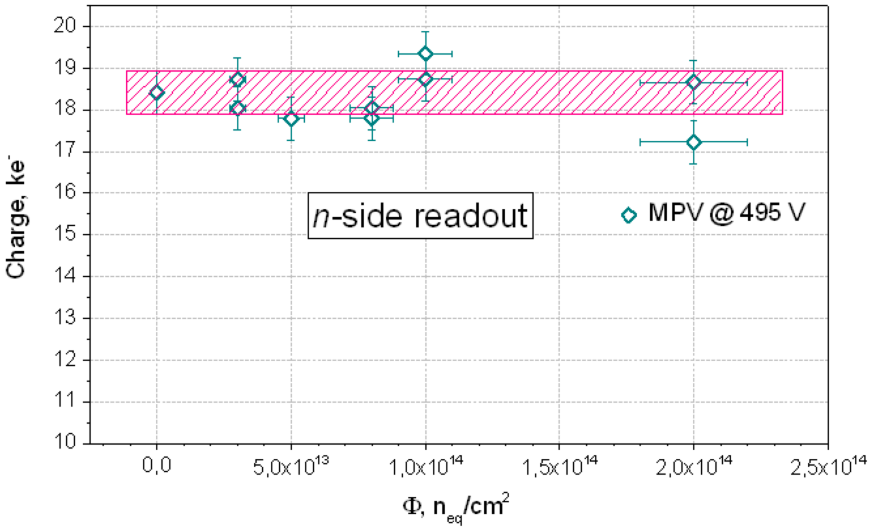

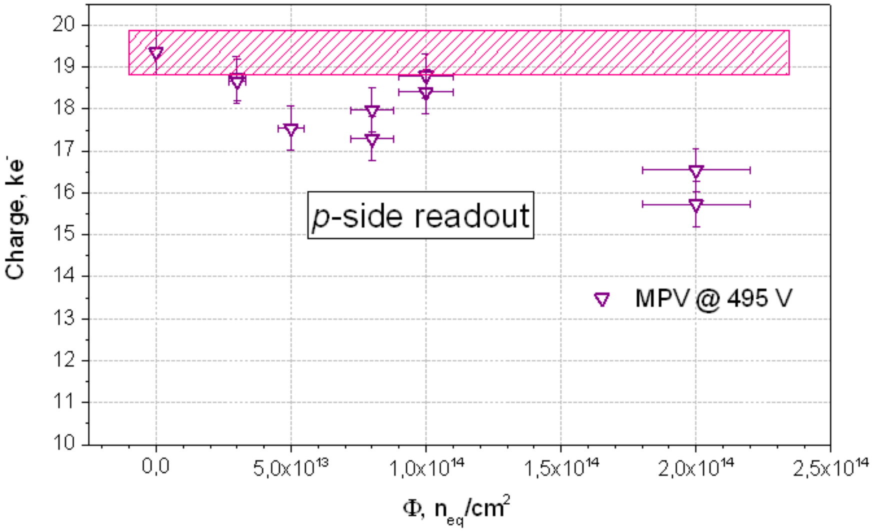

Evolution of charge collection

Measurements on **prototype sensors** (Hamamatsu and CiS, 2×10^{14} n_{eq} cm^{-2}):

- » Before irradiation: thicker sensors → higher charge collection;
- » After irradiation: relative charge collection efficiency higher for thinner detector: ≈ 80÷90% vs. ≈ 70÷80%;
- » Drift length: $L_{e,h} = (\mu\tau)_{e,h}E$;
- » Overall CCE at twice the lifetime fluence is good → S/N to be evaluated;
- » 4 detectors, all different: more statistics;
- » Measurement conditions for comparison?

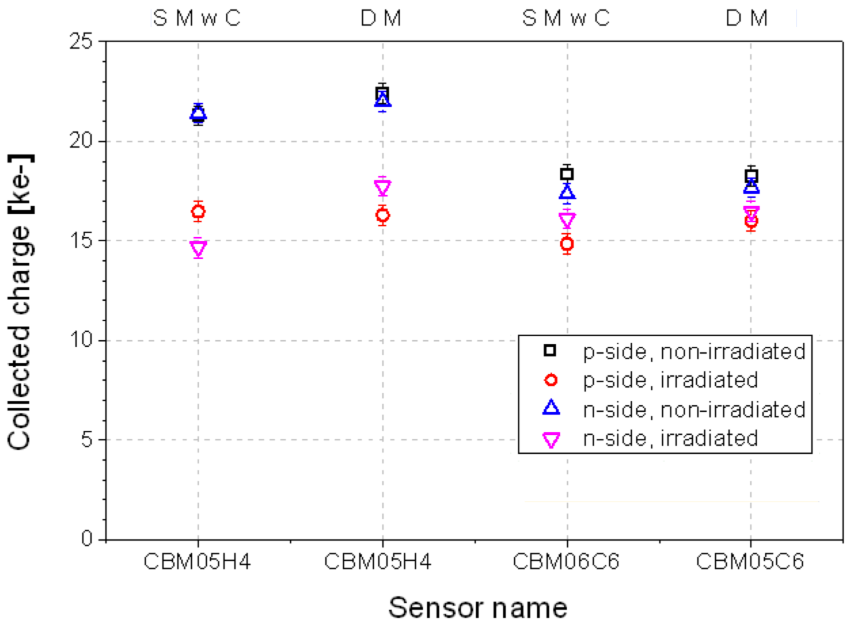

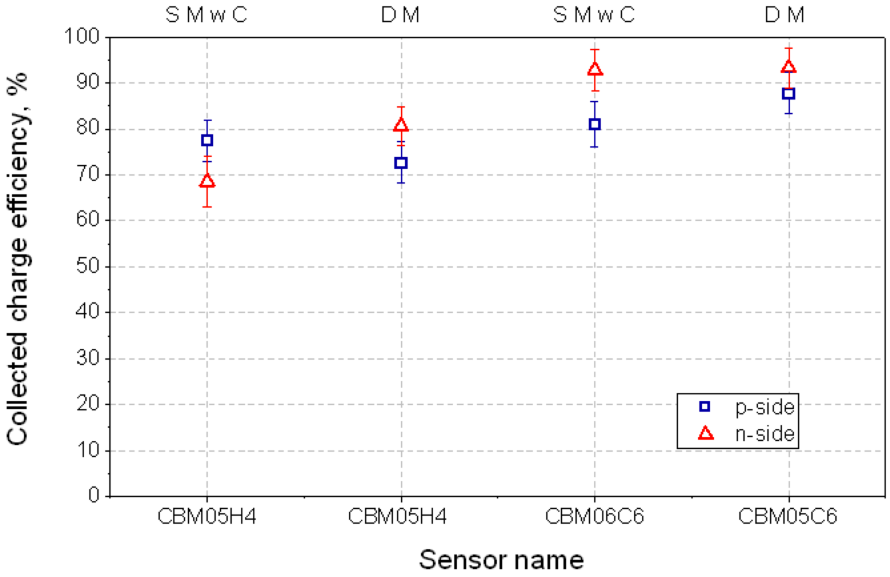

Time evolution of *V_{fd}*

Measurements on **baby sensors**:

- » higher fluence → higher effect of annealing: $N_A \sim \Phi_{eq}$, $N_Y \sim \Phi_{eq}$;
- » $w6sn2_{1e14}$ → beneficial annealing at 11 mins @ 80 ºC; $w25_{1e13}$, $w12sn2_{5e14}$: effect not pronounced;
- » $w6sn1_{1e14}$: minimum of V_{fd} after 7 days of 25 ºC exposure;
- » reverse annealing: V_{fd} before the SCSI decreases (w25), after the SCSI increases (w12sn2, w6sn2, w6sn1);
- » real conditions: maintenance period (room temperatures? 10 ºC? how long? - open).

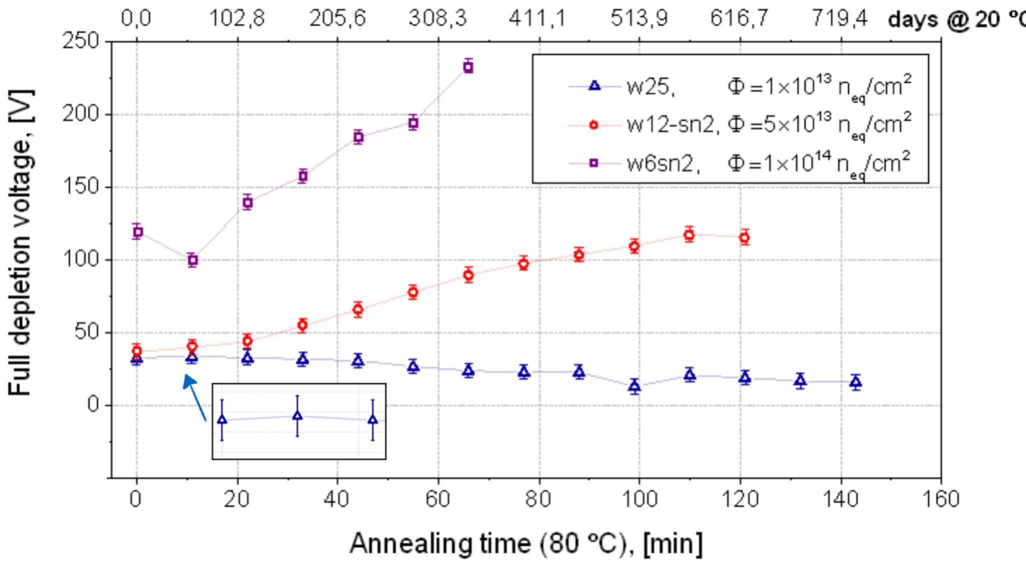

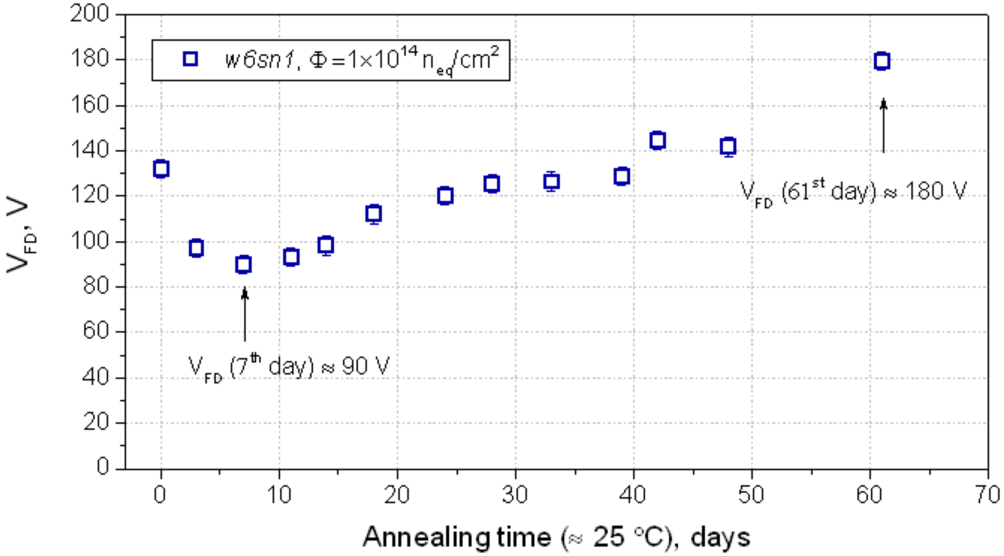

Time evolution of V_{fd} : parametrization in terms of N_{eff}

Change in absolute effective impurity concentration **(baby sensors)**:

$$\Delta N_{eff}(\Phi_{eq},t) = N_C(\Phi_{eq},t) + N_A(\Phi_{eq},t) + N_Y(\Phi_{eq},t)$$

- » Calculation describes well the data;
- » Equivalent exposure time at 20 °C is given in the upper X axis;
- » Locations of minimums via model: between the experimental points;
- » $t_{a,min(80)}$ = 6 mins; $t_{a,min(25)}$ = 5 days;
- » calculation at various temperatures → time constants from the Arrhenius equation:

$$\frac{1}{\tau_{a(Y)}} = k_{0a(0Y)} \exp\left(-\frac{E_{aa(Y)}}{k_B T_a}\right)$$

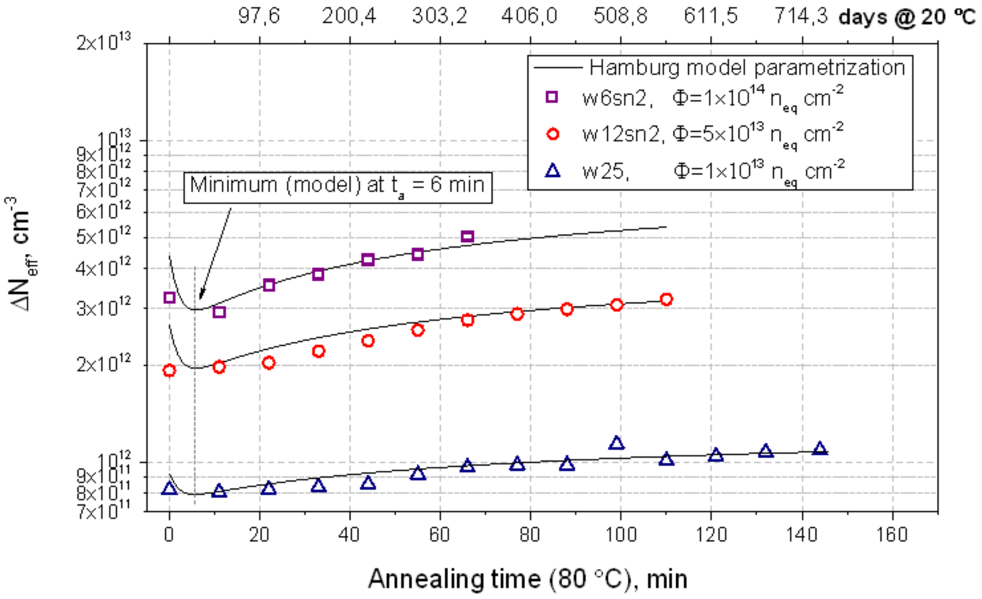

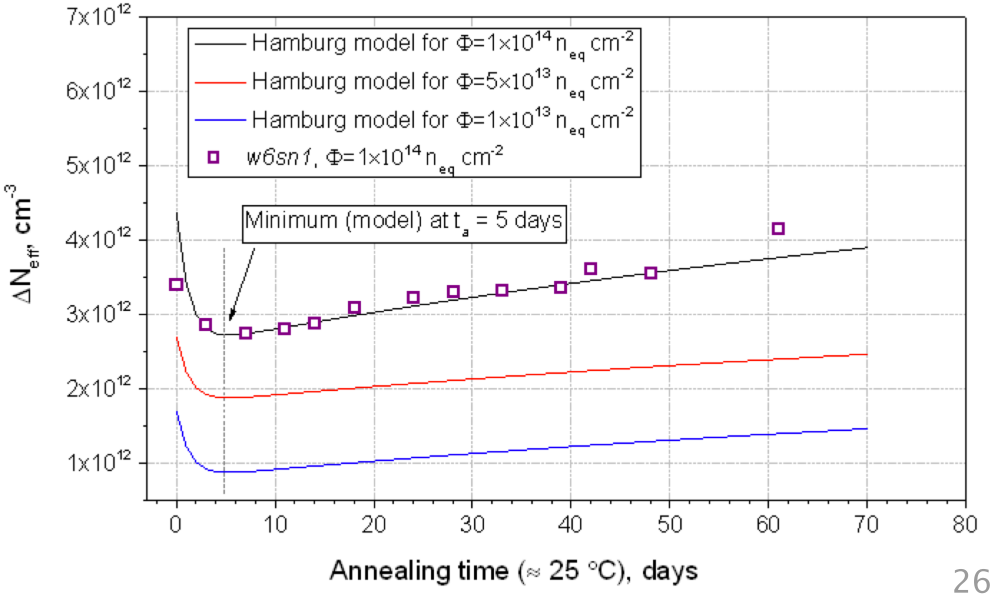

Charge collection as a function of time

Changes in charge collection **(baby sensors)**:

- Good to observe on the long-term scale with accelerated annealing;
- Either within the error bars or slow decrease;
- Even if overkept at room temperatures → *not so harmful*;
- Increasing V_{fd} may influence → lower $E(x)$ at a fixed voltage;
- Short-term scale benefits? more data needed, as 1 min. at 80 ºC = 5.14 days at 20 ºC; step = 11 min.
- Some works: CCE decreased during short-term annealing (S. Martí i García), some other works: same signal at lower applied voltages.

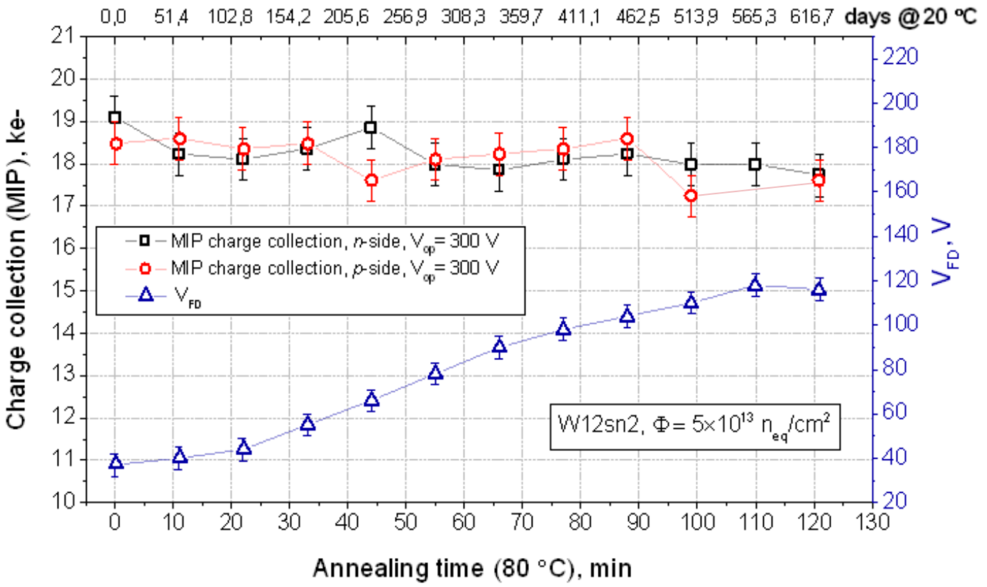

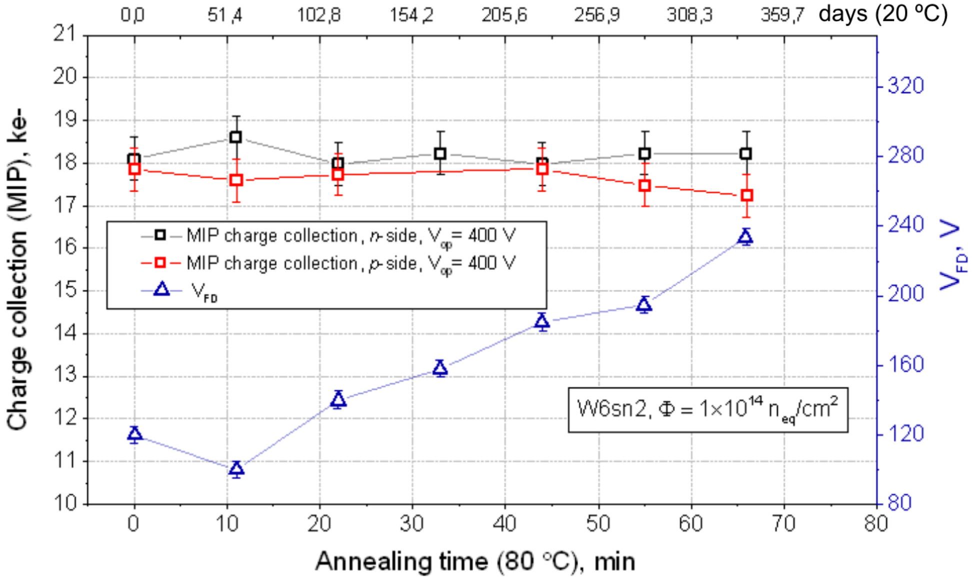

Operational stability

Operational stability:

- stable environment → stable operation;
- $I_{350\text{ V shown before}} = 0.8$ mA, $I_{\text{stabilized after the ramp-up}} = 1.4 \div 1.5$ mA;
- Slow decrease of the reverse current: can be annealing;
- Rapid increase of humidity → rapid increase of the reverse current → thermal runaway starts at some point (~ 2 mA) → ramp-down or ☠; more pronounced for CiS sensors, especially DSDM one;
- Hamamatsu sensors: full or partial recovery;

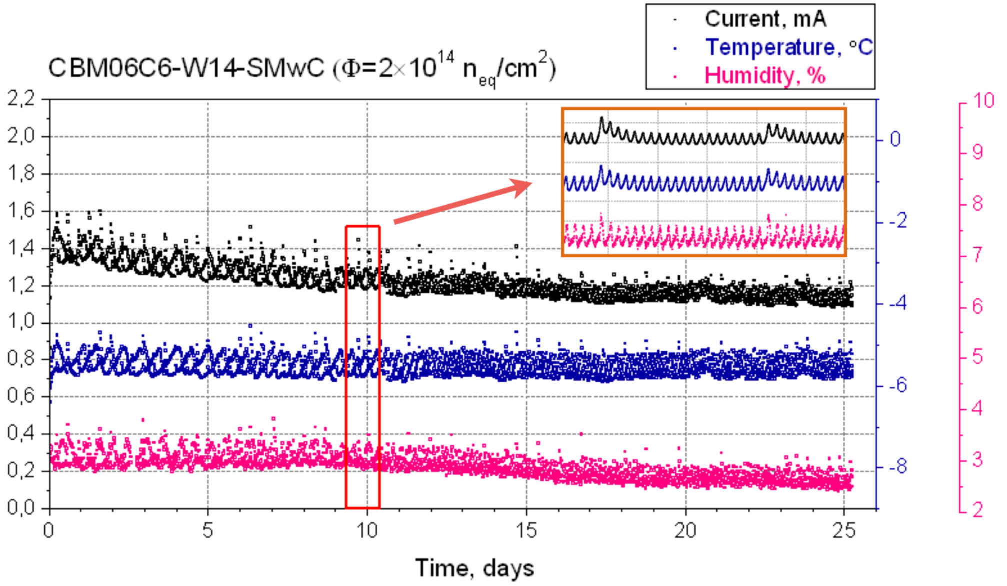

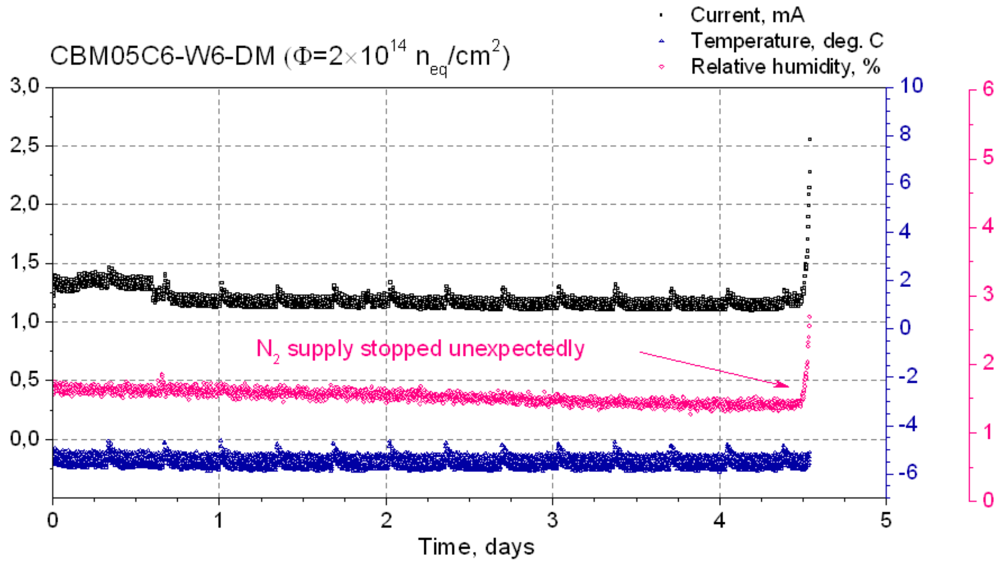

Operational stability

Operational stability:

- stable environment → stable operation;
- $I_{\text{350 V shown before}} = 0.8$ mA,
  $I_{\text{stabilized after the ramp-up}} = 1.4 \div 1.5$ mA;
- Slow decrease of the reverse current: can be annealing;
- Rapid increase of humidity → rapid increase of the reverse current → thermal runaway starts at some point (~ 2 mA) → ramp-down or ☠; more pronounced for CiS sensors (larger area, most probably), especially DSDM one;
- Hamamatsu sensors: full or partial recovery, no runaway no breakdown;
- Humidity sensitivity → not a radiation-induced effect, observed on non-irradiated sensor.

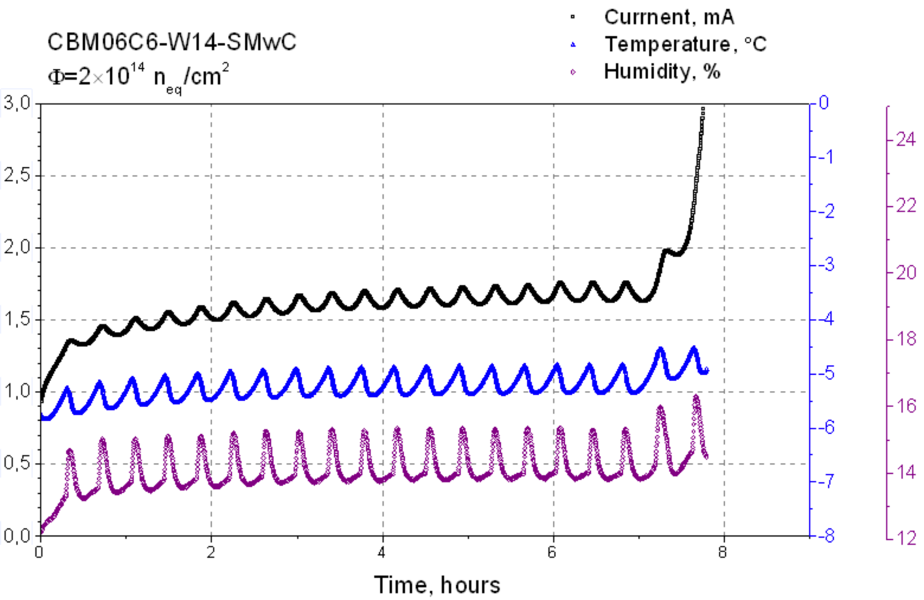

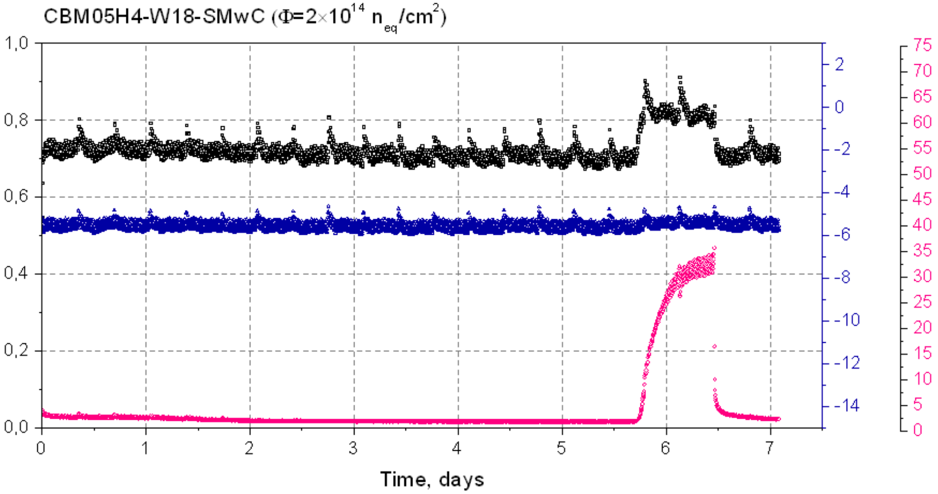

Summary

Irradiation studies:

- Charge collection (baby sensors) up to 1×10^{14} n_{eq} cm^{-2}: ≈ 95% at the *n*-side, ≈ 90% at the *p*-side → very good ;
- Charge collection of prototype sensors (CiS and Hamamatsu) at 2×10^{14} cm^{-2}: ≈ 70÷80% Hamamatsu, ≈ 80÷90 CiS;
- Charge collection as a function of time: a few percent decrease on a long-term scales (1 year and more at 20 ºC, at fixed bias voltage);
- I_{leak}, N_{eff}, V_{fd} time evolutions: understood, parameters obtained → predictions can be made;
- Operational stability: stable even at high reverse currents (~1.5 mA) under stable environmental conditions; sensitive to rapid change in humidity → synchronize monitoring and ramping-down soft;
- Next step: evaluation of the module performance (latest prototype components).

Development of the Quality Assurance test stand for strip diagnostics

Quality Assurance (QA) of the STS sensors

- Large volume production - 900 sensors to be produced;
- Double-sided sensors (2048 strips) → complicated manufacturing → increased risk of fabrication defects;
- Ensure sensor quality → Quality Assurance procedures/tests;
- QA tests to be performed: at vendor sites + at Quality Test Centres;
- Sensor quality to be monitored at several steps of the detector assembly.

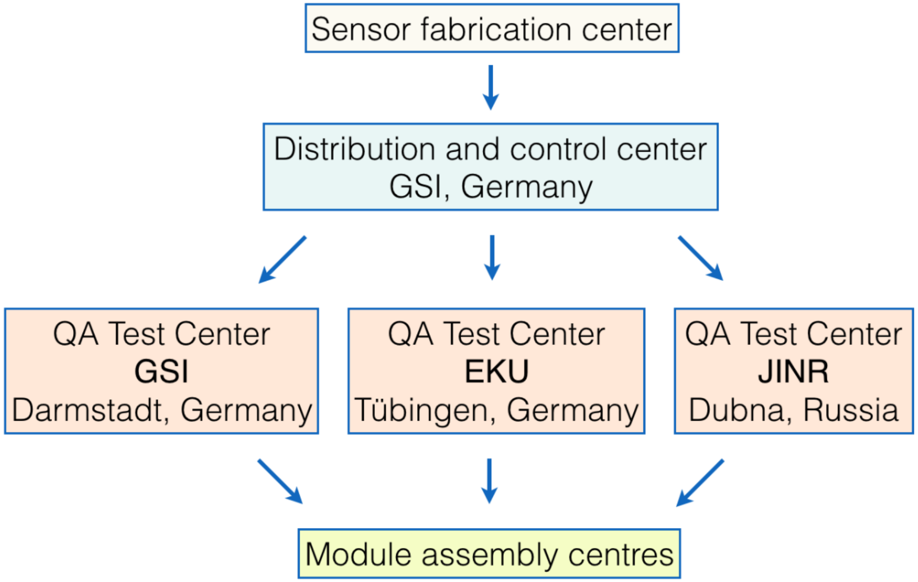

Sensor fabrication center

Distribution and control center
GSI, Germany

QA Test Center
GSI
Darmstadt, Germany

QA Test Center
EKU
Tübingen, Germany

QA Test Center
JINR
Dubna, Russia

Module assembly centres

Quality Assurance (QA) of the STS sensors

- Large volume production - 900 sensors to be produced;
- Double-sided sensors (2048 strips) → complicated manufacturing → increased risk of fabrication defects;
- Ensure sensor quality → Quality Assurance procedures/tests;
- QA tests to be performed: at vendor sites + at Quality Test Centres;
- Sensor quality to be monitored at several steps of the detector assembly.

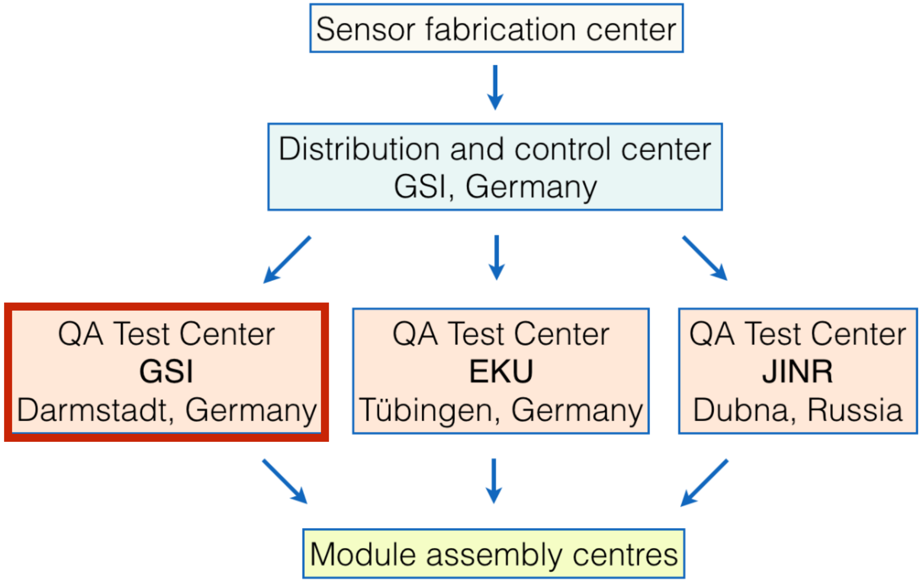

Sensor fabrication center

Distribution and control center
GSI, Germany

QA Test Center
GSI
Darmstadt, Germany

QA Test Center
EKU
Tübingen, Germany

QA Test Center
JINR
Dubna, Russia

Module assembly centres

Quality Assurance tests

- QA tests on a sensor level: determine the overall sensor health;

- QA tests on a strip level:

  » determine the design parameters (microscopic electrical tests);

  » evaluate the strip quality (strip diagnostic tests).

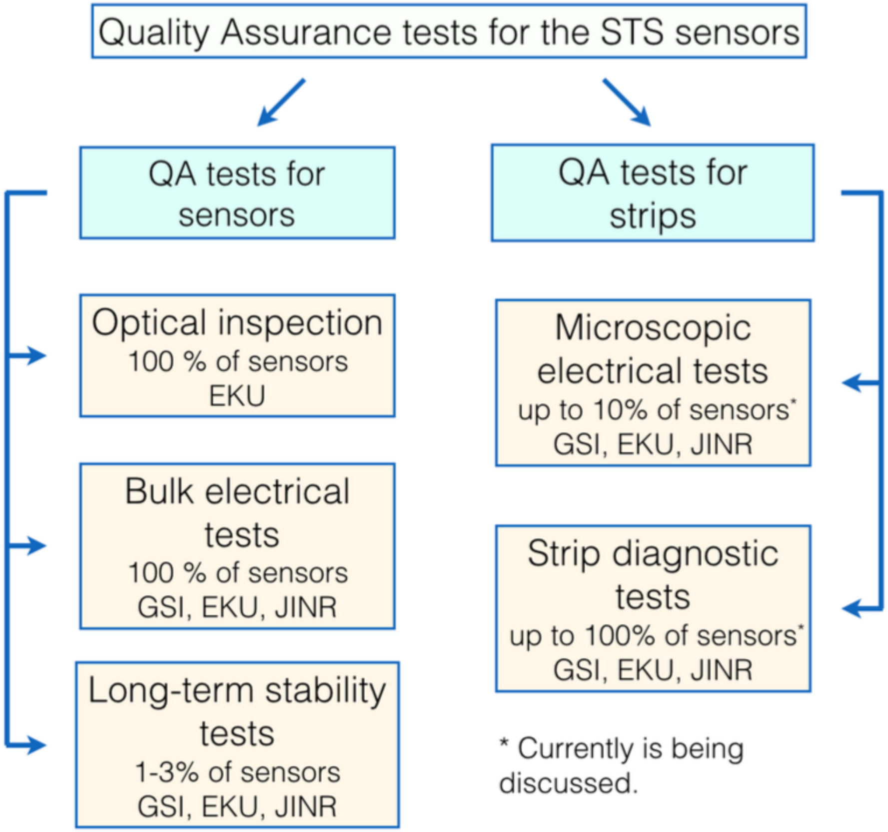

Quality Assurance tests for the STS sensors

QA tests for sensors

QA tests for strips

Optical inspection
100 % of sensors
EKU

Bulk electrical tests
100 % of sensors
GSI, EKU, JINR

Long-term stability tests
1-3% of sensors
GSI, EKU, JINR

Microscopic electrical tests
up to 10% of sensors*
GSI, EKU, JINR

Strip diagnostic tests
up to 100% of sensors*
GSI, EKU, JINR

* Currently is being discussed.

Quality Assurance tests

- QA tests on a sensor level: determine the overall sensor health;

- QA tests on a strip level:

  » determine the design parameters (microscopic electrical tests);

  » evaluate the strip quality (strip diagnostic tests).

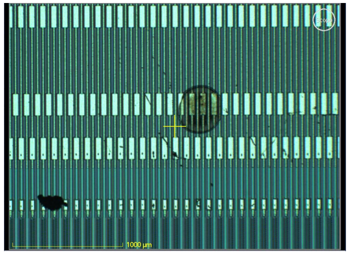

Visual inspection

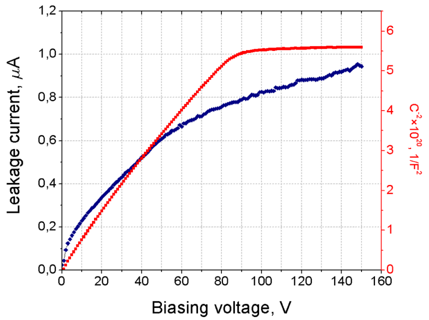

IV, CV test

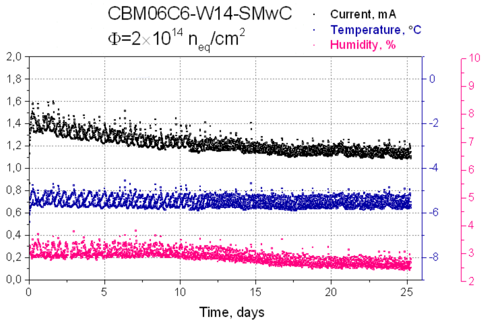

Long-term stability test

Quality Assurance tests

- QA tests on a sensor level: determine the overall sensor health;

- QA tests on a strip level:

  » determine the design parameters (microscopic electrical tests);

  » evaluate the **strip quality (strip diagnostic tests).**

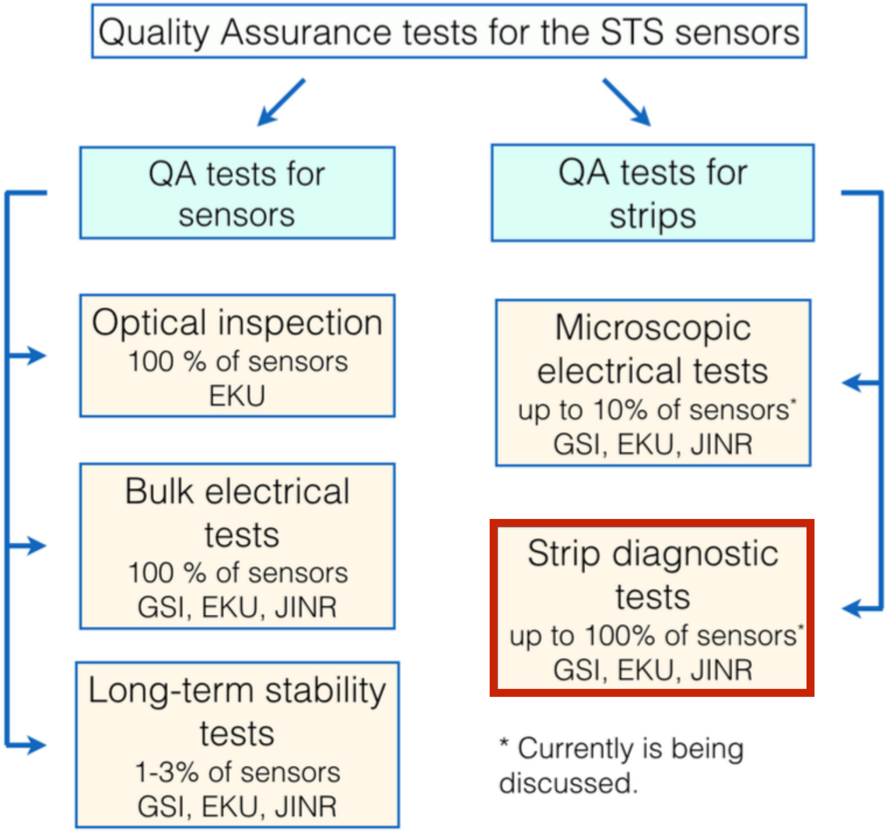

Quality Assurance tests for the STS sensors

QA tests for sensors

QA tests for strips

Optical inspection
100 % of sensors
EKU

Bulk electrical tests
100 % of sensors
GSI, EKU, JINR

Long-term stability tests
1-3% of sensors
GSI, EKU, JINR

Microscopic electrical tests
up to 10% of sensors*
GSI, EKU, JINR

Strip diagnostic tests
up to 100% of sensors*
GSI, EKU, JINR

* Currently is being discussed.

Strip diagnostic tests

- Evaluate strip quality → identify strip faults;
- Strip faults: danger for the readout electronics; deteriorate track reconstruction efficiency;
- Most common strip faults (STS sensors): **“pinholes”, readout strip short circuits.**
- To be measured additionally: **strip leakage current**; “leaky” strips → potential damage to the r/o electronics;
- **Scratches** → very high risk of strip faults.

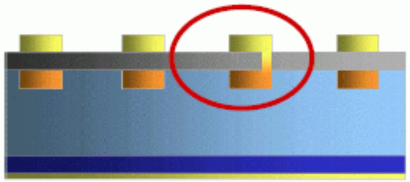

“Pinhole”

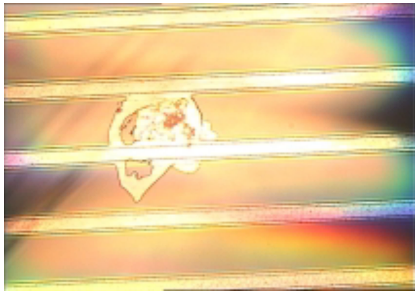

Readout strip “short”

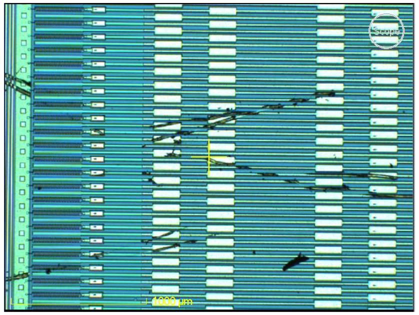

Surface scratches

Strip diagnostic tests

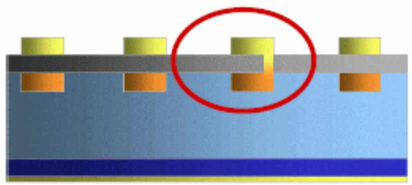

“Pinhole”

Series production: 2048 strips per sensor → 1 843 200 strips (900 sensors) → automation required.

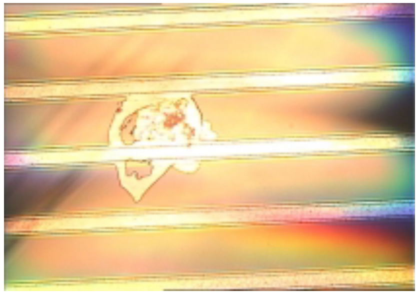

Readout strip “short”

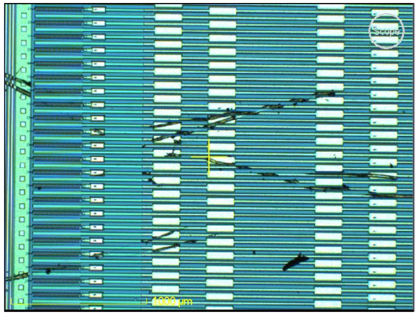

Surface scratches

Equipment

- Cleanroom: class ISO 4;
- Süss PA300 PS wafer prober
  - » ~ 1 µm movement precision;
  - » Control center, GUI;
- Measurement instruments: Keithley 2410, Keithley 6487, QuadTech 7600;
- Manual measurements.

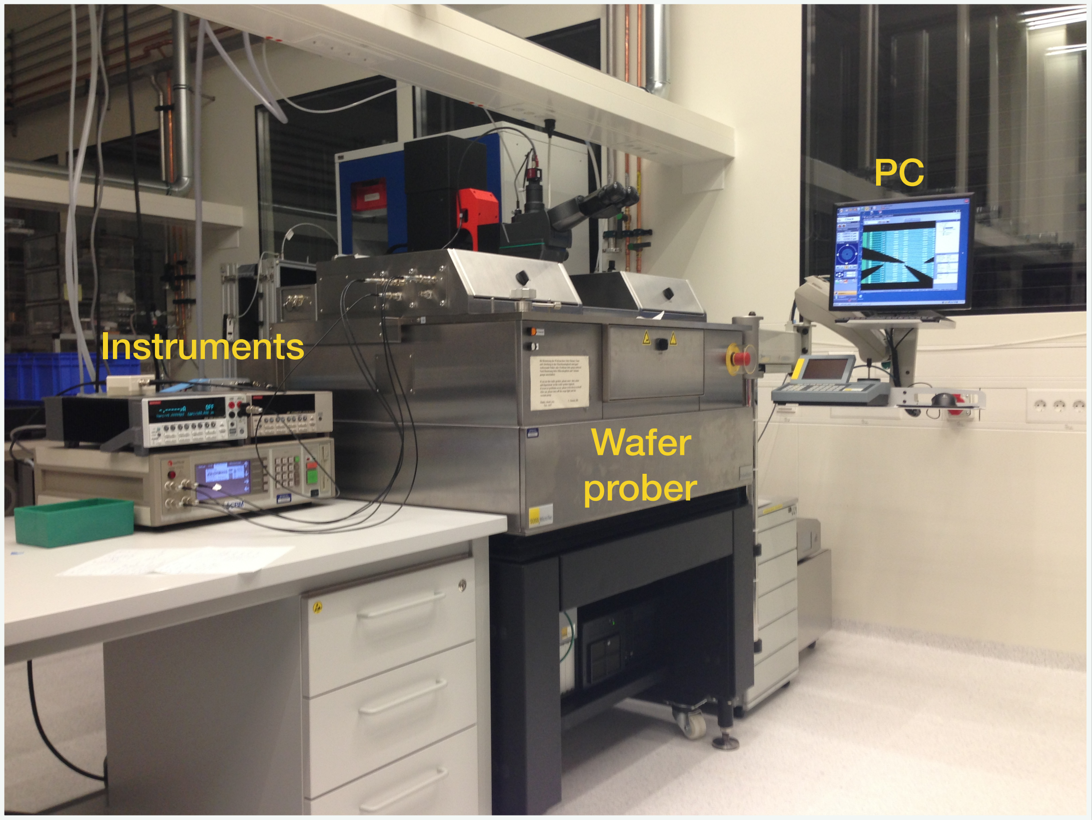

Cleanroom lab @ GSI, Darmstadt

How the strip diagnostic tests are done

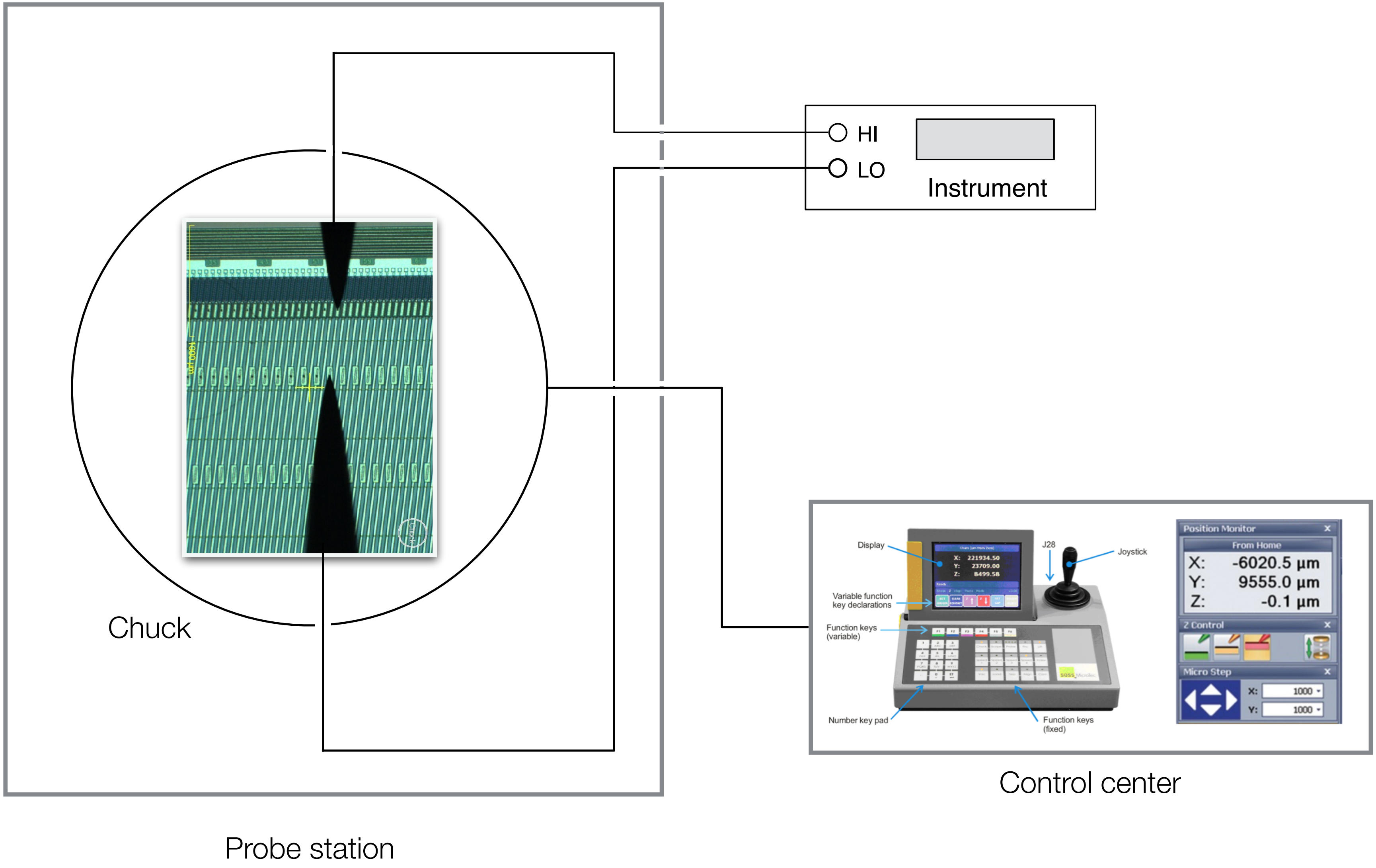

X: 221934.50
Y: 23709.00
Z: 8499.58

From Home
X: -6020.5 µm
Y: 9555.0 µm
Z: -0.1 µm

X: 1000
Y: 1000

Concept of the automated test stand

- Requires simultaneous control of the instruments and the probe station electronics;
- Decouple the tasks: Master and Slave (practical reasons);
- LabView software for initialization, measurement flow, communication, automation.

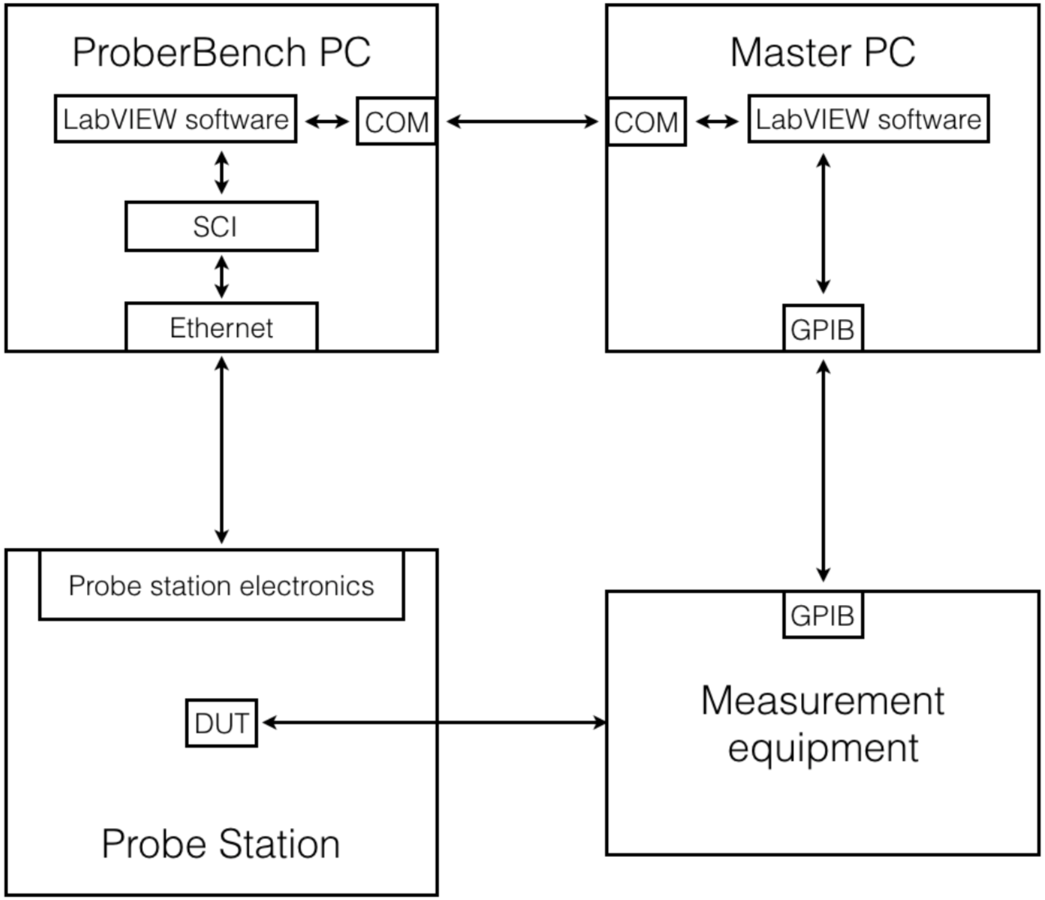

Realization: step by step

- Automation of the stepping procedure;
- Virtual instruments and interface developed for pinhole and readout strip short circuit tests (LabView);
- Added: strip leakage current test;
- Next: multi-purpose measurements.

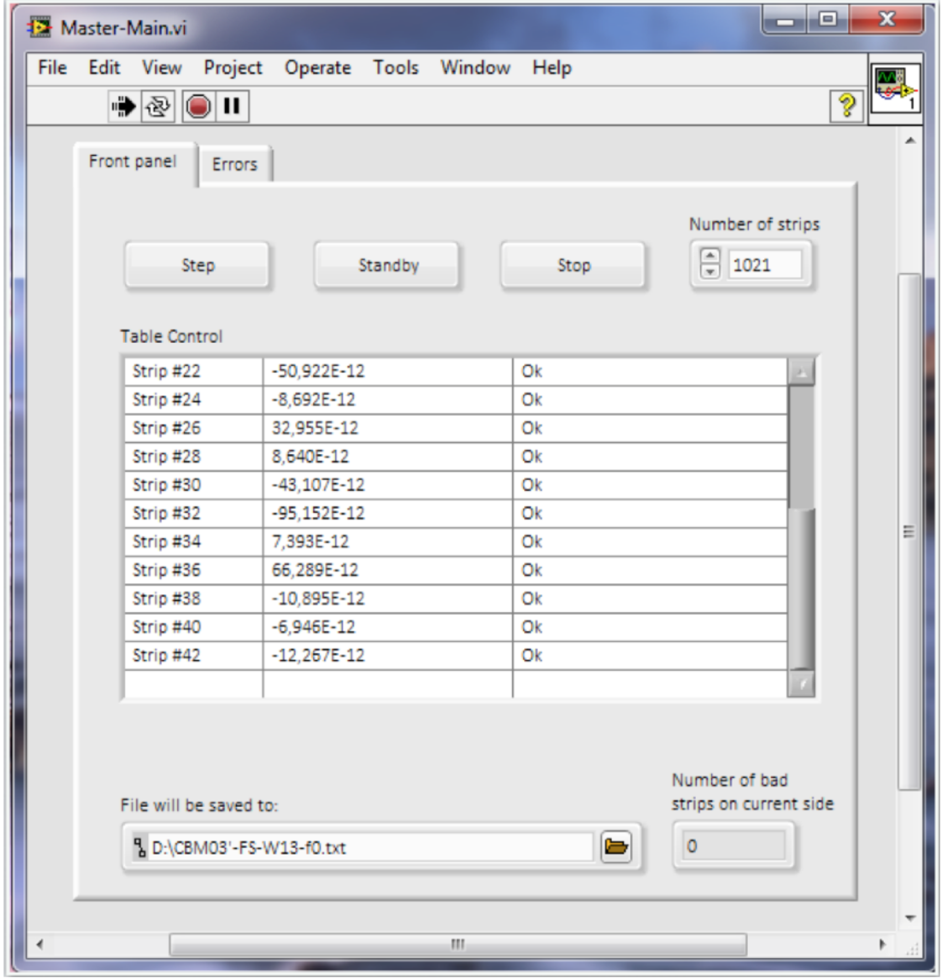

Number of strips: 1021

Table Control

Strip #22	-50,922E-12	Ok
Strip #24	-8,692E-12	Ok
Strip #26	32,955E-12	Ok
Strip #28	8,640E-12	Ok
Strip #30	-43,107E-12	Ok
Strip #32	-95,152E-12	Ok
Strip #34	7,393E-12	Ok
Strip #36	66,289E-12	Ok
Strip #38	-10,895E-12	Ok
Strip #40	-6,946E-12	Ok
Strip #42	-12,267E-12	Ok

File will be saved to: D:\CBM03'-FS-W13-f0.txt

Number of bad strips on current side: 0

Switching matrix: multi-purpose measurements

- Switching matrix (multiplexer): links any input with any output;
- Using various needle combinations → various tests can be done in a row;
- Measurement time is reduced;
- Probing of the pads: minimized → risk of scratching minimized;
- Matrix chosen: Keithley 708B mainframe + 7072-HV switching card; 8 inputs × 12 outputs.

Switching matrix: multi-purpose measurements

- Switching matrix (multiplexer): links any input with any output;
- Using various needle combinations → various tests can be done in a row;
- Measurement time is reduced;
- Probing of the pads: minimized → risk of scratching minimized;
- Matrix chosen: Keithley 708B mainframe + 7072-HV switching card; 8 inputs × 12 outputs.
- Integrated to the setup.

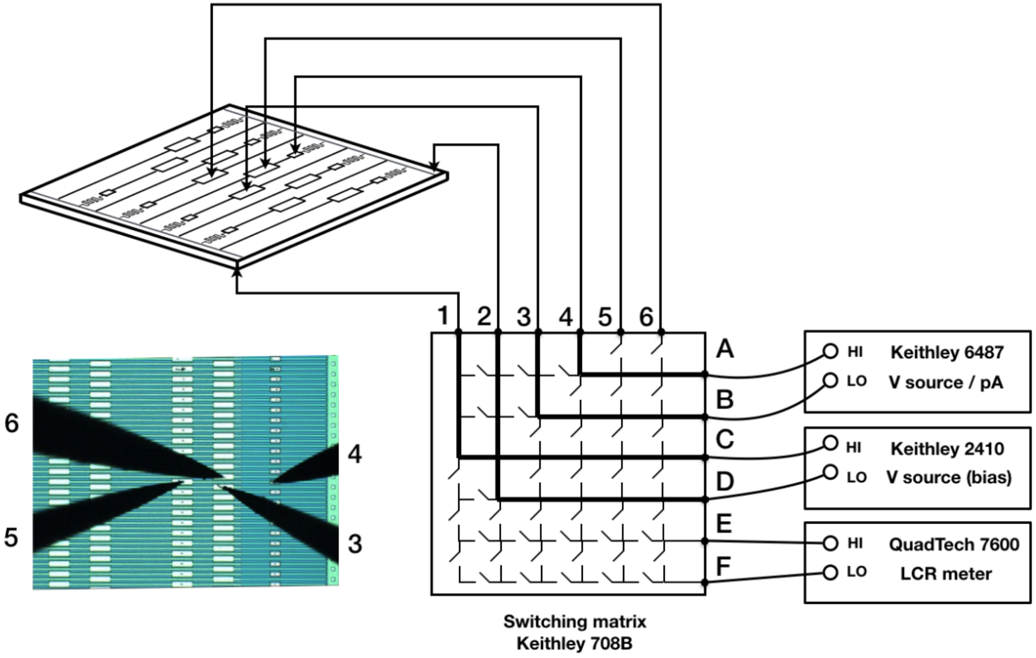

Software interface for automated tests

- Automated tests: strip diagnostic tests + coupling capacitance (optional);
- Measurement results are reflected online and stored in a file;
- Both single and multiple tests can be performed;
- Optimization of the measurement sequence and speed;
- Three diagnostic tests: ~ 4 seconds per strip.

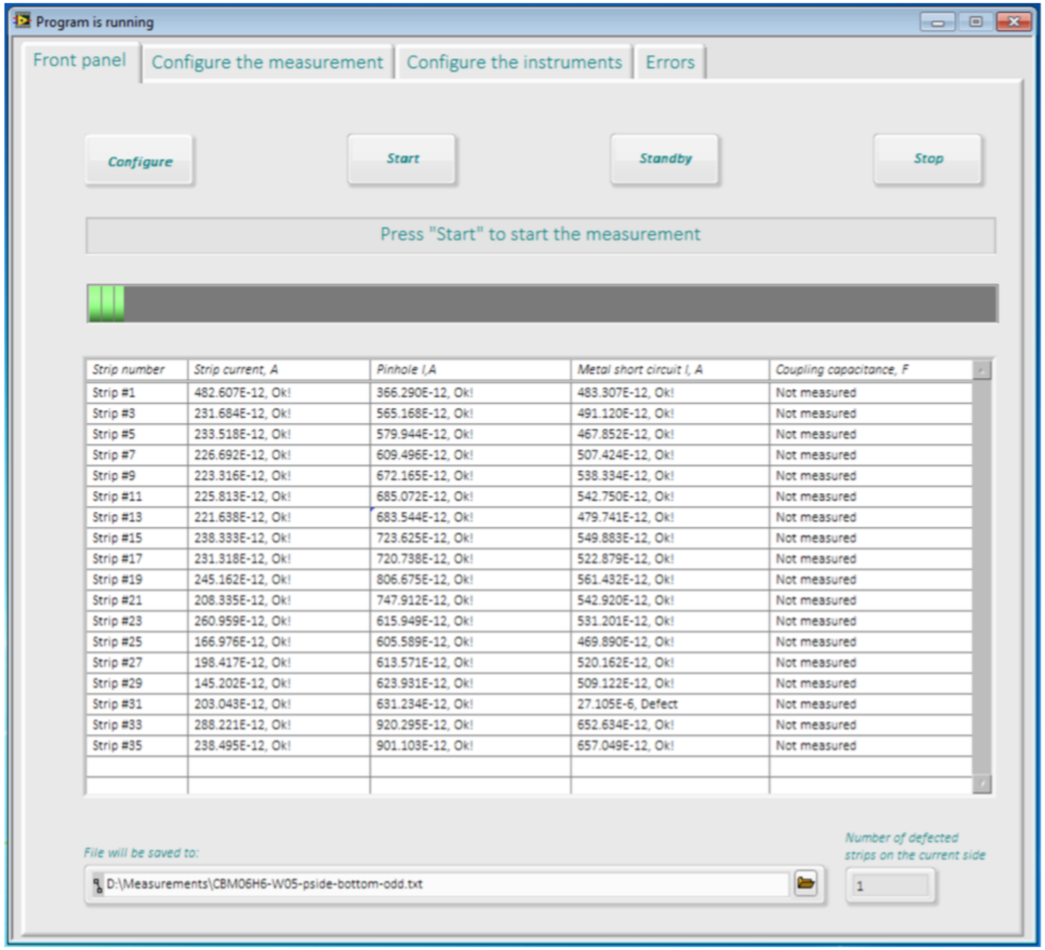

Press "Start" to start the measurement

Strip number	Strip current, A	Pinhole I,A	Metal short circuit I, A	Coupling capacitance, F
Strip #1	482.607E-12, Ok!	366.290E-12, Ok!	483.307E-12, Ok!	Not measured
Strip #3	231.684E-12, Ok!	565.168E-12, Ok!	491.120E-12, Ok!	Not measured
Strip #5	233.518E-12, Ok!	579.944E-12, Ok!	467.852E-12, Ok!	Not measured
Strip #7	226.692E-12, Ok!	609.496E-12, Ok!	507.424E-12, Ok!	Not measured
Strip #9	223.316E-12, Ok!	672.165E-12, Ok!	538.334E-12, Ok!	Not measured
Strip #11	225.813E-12, Ok!	685.072E-12, Ok!	542.750E-12, Ok!	Not measured
Strip #13	221.638E-12, Ok!	683.544E-12, Ok!	479.741E-12, Ok!	Not measured
Strip #15	238.333E-12, Ok!	723.625E-12, Ok!	549.883E-12, Ok!	Not measured
Strip #17	231.318E-12, Ok!	720.738E-12, Ok!	522.879E-12, Ok!	Not measured
Strip #19	245.162E-12, Ok!	806.675E-12, Ok!	561.432E-12, Ok!	Not measured
Strip #21	208.335E-12, Ok!	747.912E-12, Ok!	542.920E-12, Ok!	Not measured
Strip #23	260.959E-12, Ok!	615.949E-12, Ok!	531.201E-12, Ok!	Not measured
Strip #25	166.976E-12, Ok!	605.589E-12, Ok!	469.890E-12, Ok!	Not measured
Strip #27	198.417E-12, Ok!	613.571E-12, Ok!	520.162E-12, Ok!	Not measured
Strip #29	145.202E-12, Ok!	623.931E-12, Ok!	509.122E-12, Ok!	Not measured
Strip #31	203.043E-12, Ok!	631.234E-12, Ok!	27.105E-6, Defect	Not measured
Strip #33	288.221E-12, Ok!	920.295E-12, Ok!	652.634E-12, Ok!	Not measured
Strip #35	238.495E-12, Ok!	901.103E-12, Ok!	657.049E-12, Ok!	Not measured

File will be saved to: D:\Measurements\CBM06H6-W05-pside-bottom-odd.txt

Number of defected strips on the current side: 1

Software interface for automated tests

- Automated tests: strip diagnostic tests + coupling capacitance (optional);
- Measurement results are reflected online and stored in a file;
- Both single and multiple tests can be performed;
- Optimization of the measurement sequence and speed;
- Three diagnostic tests: ~ 4 seconds per strip.

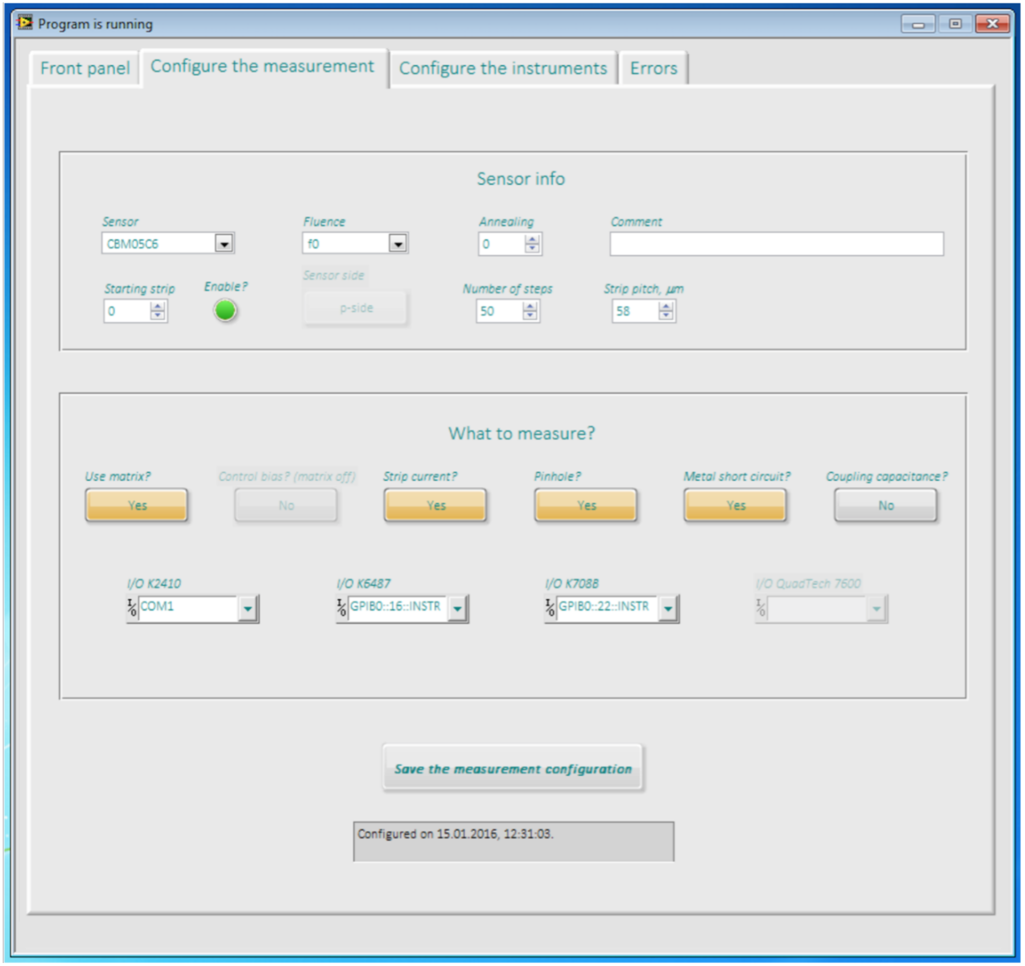

Sensor info

Sensor: CBM05C6
Fluence: f0
Annealing: 0
Comment:
Starting strip: 0
Enable? ●
Sensor side: p-side
Number of steps: 50
Strip pitch, µm: 58

What to measure?

Use matrix?: Yes
Control bias? (matrix off): No
Strip current?: Yes
Pinhole?: Yes
Metal short circuit?: Yes
Coupling capacitance?: No

I/O K2410: COM1
I/O K6487: GPIB0::16::INSTR
I/O K7088: GPIB0::22::INSTR
I/O QuadTech 7600:

Configured on 15.01.2016, 12:31:03.

Software interface for automated tests

- Automated tests: strip diagnostic tests + coupling capacitance (optional);
- Measurement results are reflected online and stored in a file;
- Both single and multiple tests can be performed;
- Optimization of the measurement sequence and speed;
- Three diagnostic tests: ~ 4 seconds per strip.

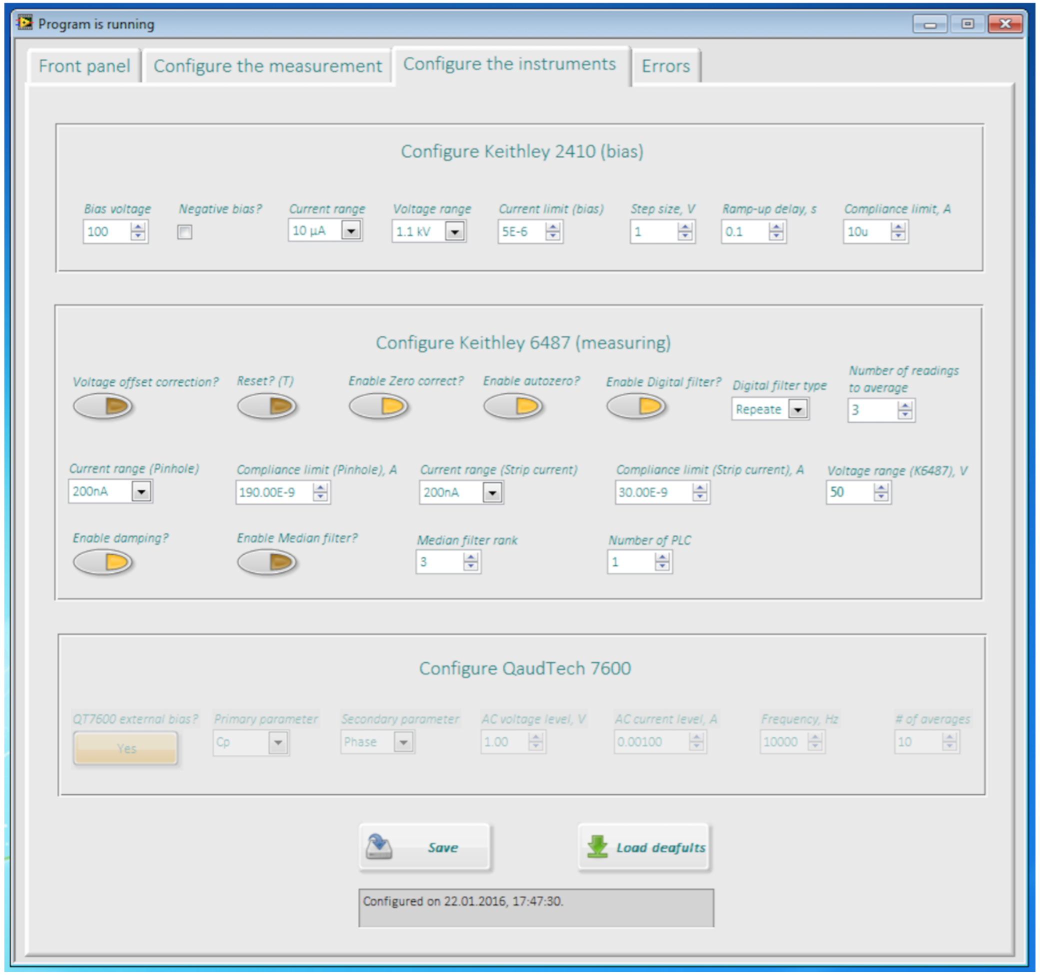

Configure Keithley 2410 (bias)

Bias voltage	Negative bias?	Current range	Voltage range	Current limit (bias)	Step size, V	Ramp-up delay, s	Compliance limit, A
100	☐	10 µA	1.1 kV	5E-6	1	0.1	10u

Configure Keithley 6487 (measuring)

Voltage offset correction?	Reset? (T)	Enable Zero correct?	Enable autozero?	Enable Digital filter?	Digital filter type	Number of readings to average
					Repeate	3

Current range (Pinhole)	Compliance limit (Pinhole), A	Current range (Strip current)	Compliance limit (Strip current), A	Voltage range (K6487), V
200nA	190.00E-9	200nA	30.00E-9	50

Enable damping?	Enable Median filter?	Median filter rank	Number of PLC
		3	1

Configure QaudTech 7600

QT7600 external bias?	Primary parameter	Secondary parameter	AC voltage level, V	AC current level, A	Frequency, Hz	# of averages
Yes	Cp	Phase	1.00	0.00100	10000	10

Configured on 22.01.2016, 17:47:30.

Typical output of the automated scan

- 3 tests performed in a row: strip leakage current, pinhole test, readout strip short test;

- ~ 4 seconds per strip (3 tests);

- 1 pinhole failure identified: strip #410;

- Other parameters: normal;

- Acceptance in terms of strip defects: < 1% per sensor (both sides);

- Sensor quality so far: < 0.3%* (CiS); < 0.7% (Hamamatsu).

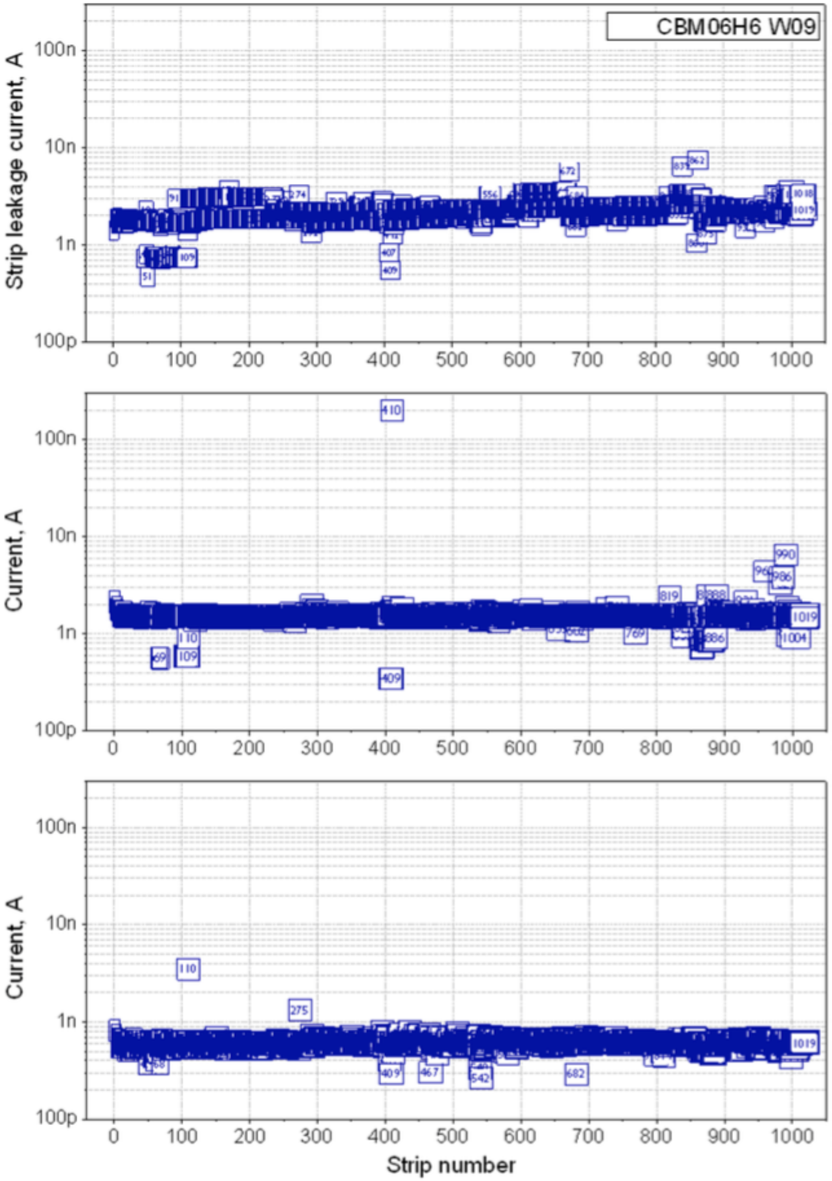

---

*Based on pinhole test data.

Summary

Quality Assurance:

- A test stand for automated strip diagnostic tests developed;
- LabView software for automation;
- Multi-purpose measurements: three QA tests are done in a row; ~4 seconds measurement time per strip;
- To be used during series production of sensors.

Summary

Quality Assurance:

- » A test stand for automated strip diagnostic tests developed;
- » LabView software for automation;
- » Multi-purpose measurements: three QA tests are done in a row; ~4 seconds measurement time per strip;
- » To be used during series production of sensors.

Thank you for attention!

Backup slides

Evolution of the full depletion voltage

Measurements with **prototype sensors (CBM05, 06)** irradiated with protons:

- *V_{fd}* was not extracted from the C-V measurement! ➝ distortion due to high leakage currents;
- Estimation of *V_{fd}* using the Hamburg model: difference for thicker (Hamamatsu) and thinner (CiS) sensors ➝ evolution is different ➝ comparison is not trivial.

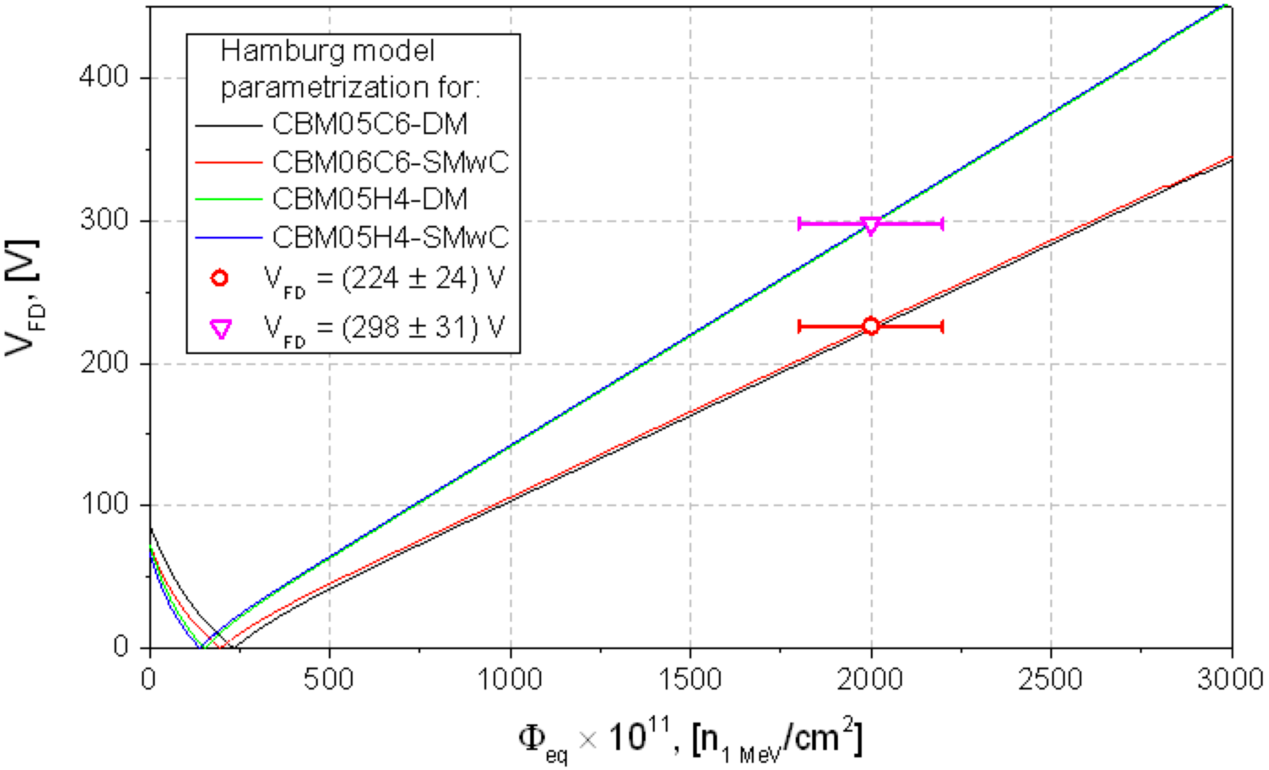

Time evolution of I_{leak}

Measurements on **baby sensors**:

- I_{leak} decreases at both 25 ºC and 80 ºC as expected;
- $\alpha_{(10/80)} = (5.32\pm0.05)\times10^{-17}$ A/cm;
- precise evolution → precise measurements with temperature compensation and suppression of the surface currents.

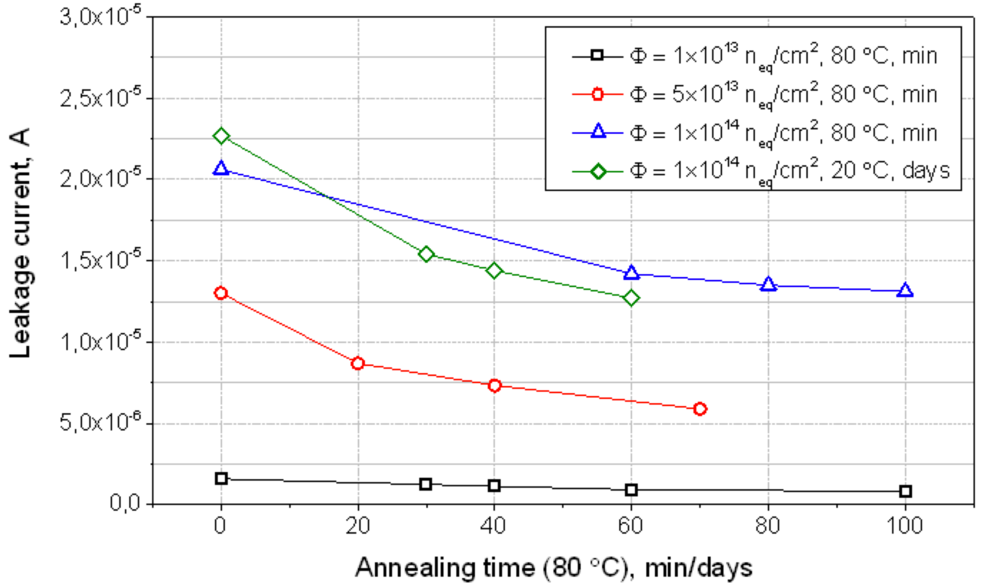

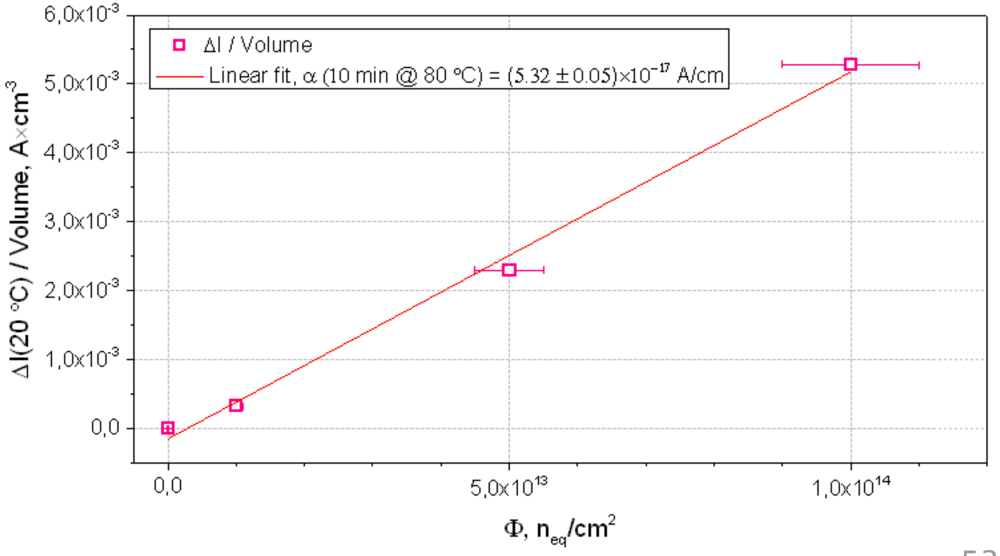

Setup (charge collection tests)

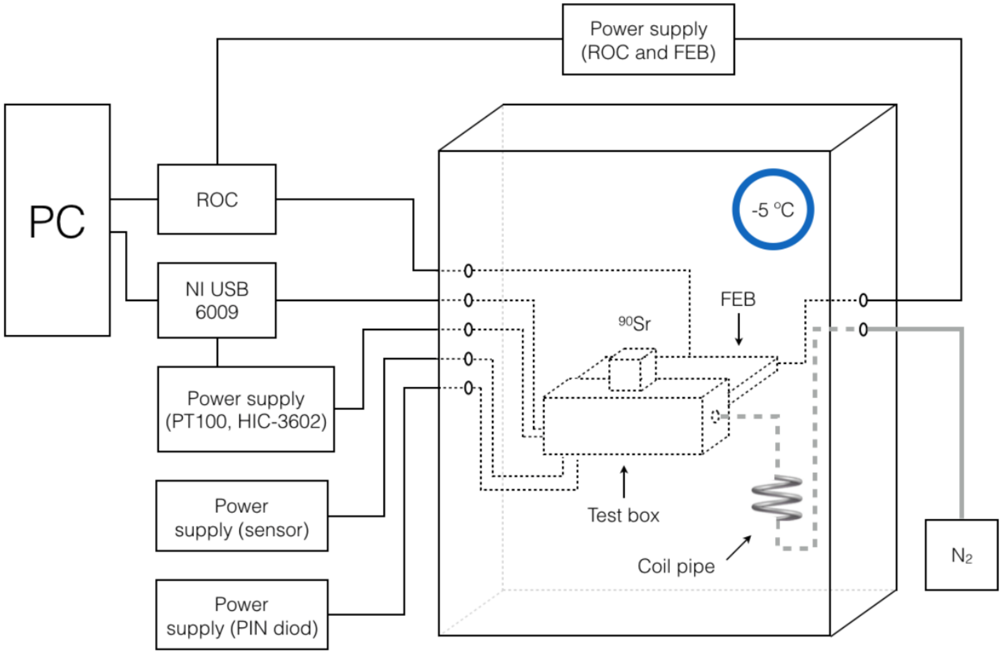

(a)

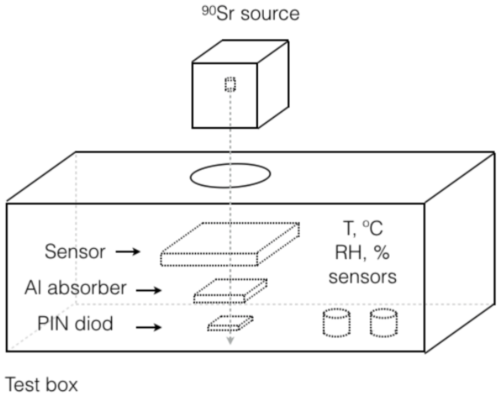

Au+Au collisions, hadronic freeze-out line

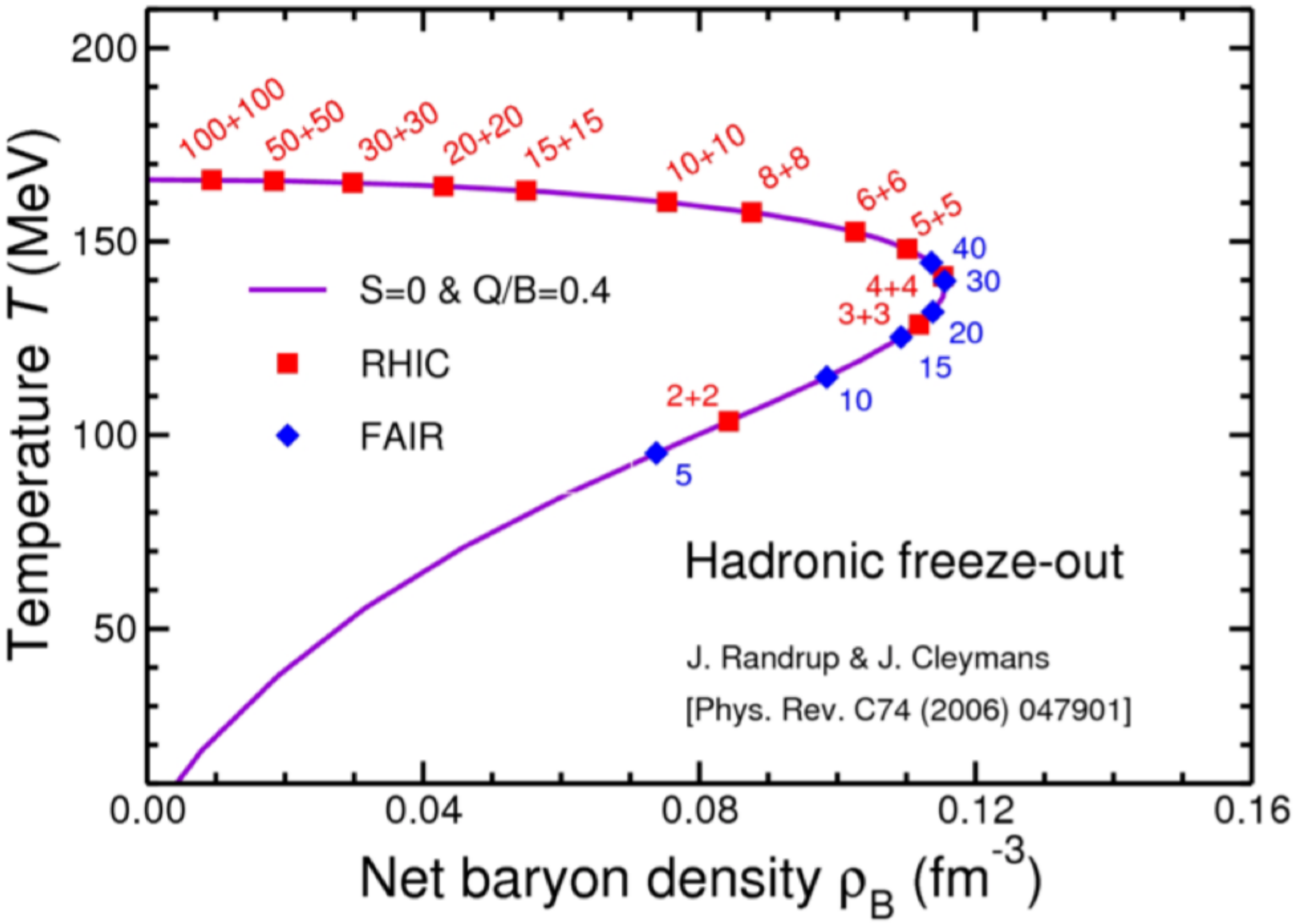

STS performance

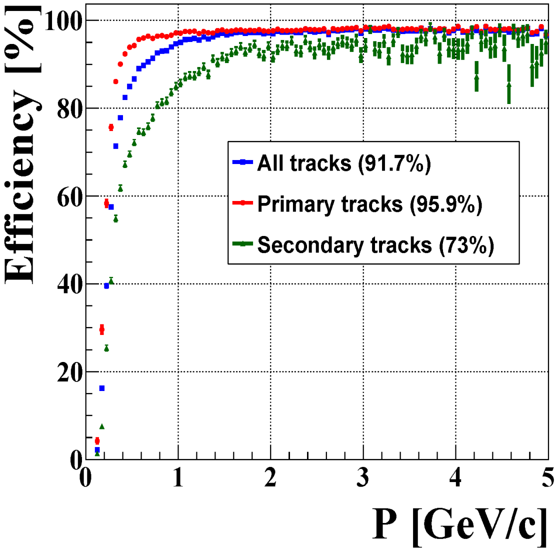

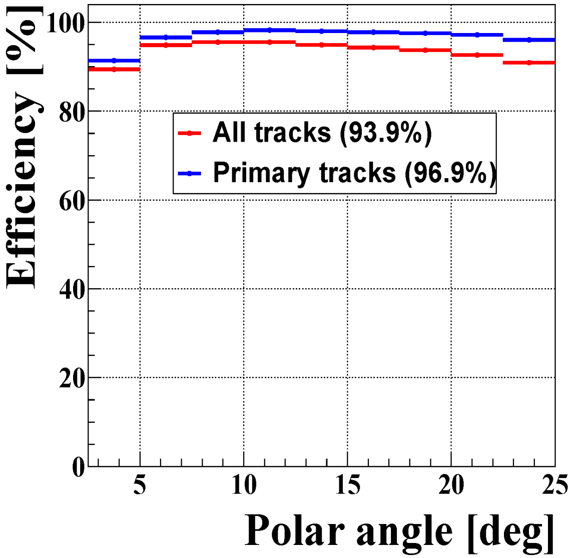

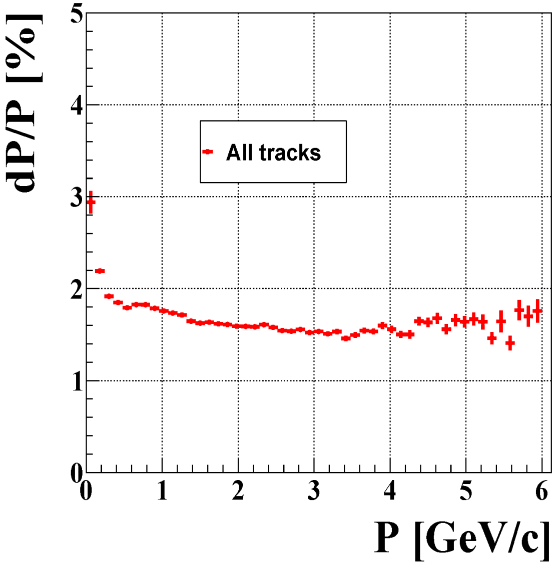

Track reconstruction efficiency

Momentum resolution

STS test socket

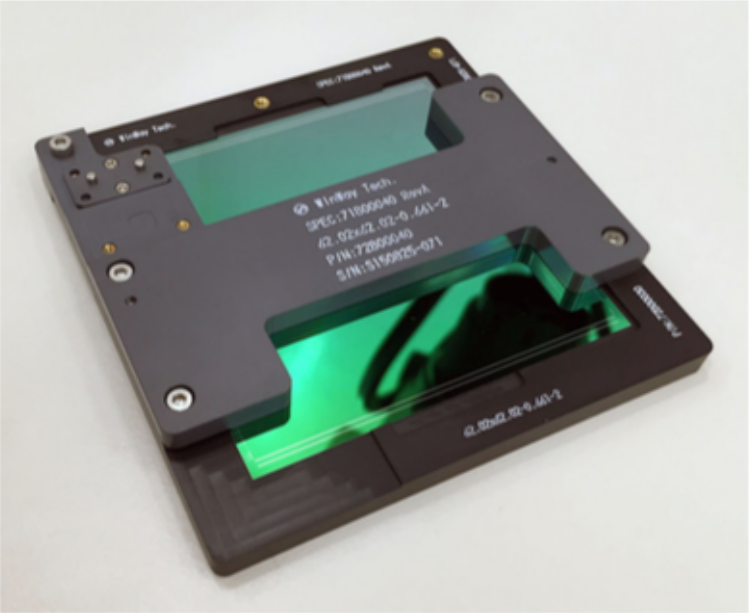

Prototype sensor mounted in the test socket

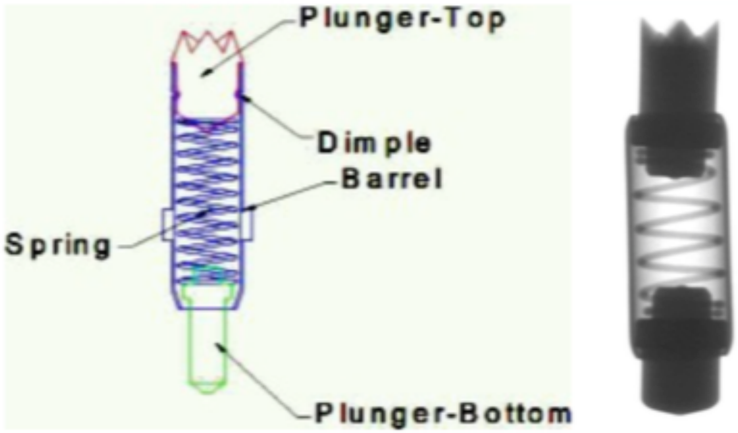

(b)

Pogo-pins

Readout electronics

- *purely data driven read-out*
- *time-stamped data elements*

STS-XYTER ASIC

128 sensor channels

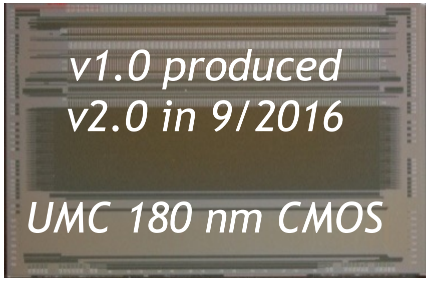

v1.0 produced
v2.0 in 9/2016

UMC 180 nm CMOS

channels	128, polarity +/-
noise	< 1ke$^-$ at 20-50pF load
ADC range	linear up to12 fC, 5 bit
clock	250 MHz
power	< 10 mW/channel
timestamp	< 10 ns resolution
out interface	5 × 500 Mbit/s LVDS

Front-end Board

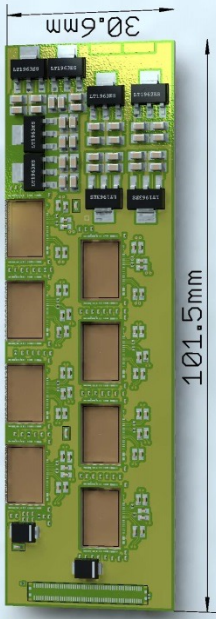

time-stamped data

8 STS-XYTER chips
à 1/2/5 LVDS links out

under development

copper link

Read-Out Board

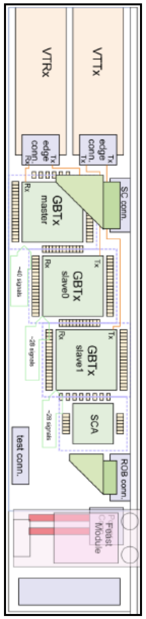

data combining

GBTx chip-set (CERN):
3 GBTx, 1 VTRx, 1 VTTx, 1 SCA

42 E-links à 320 Mb/s
3 GBT optical uplinks à 4.48 Gb/s

under development / production

optical link

Data Processing Board
time-slicing

FLES farm
online event computing

STS-XYTER: structure

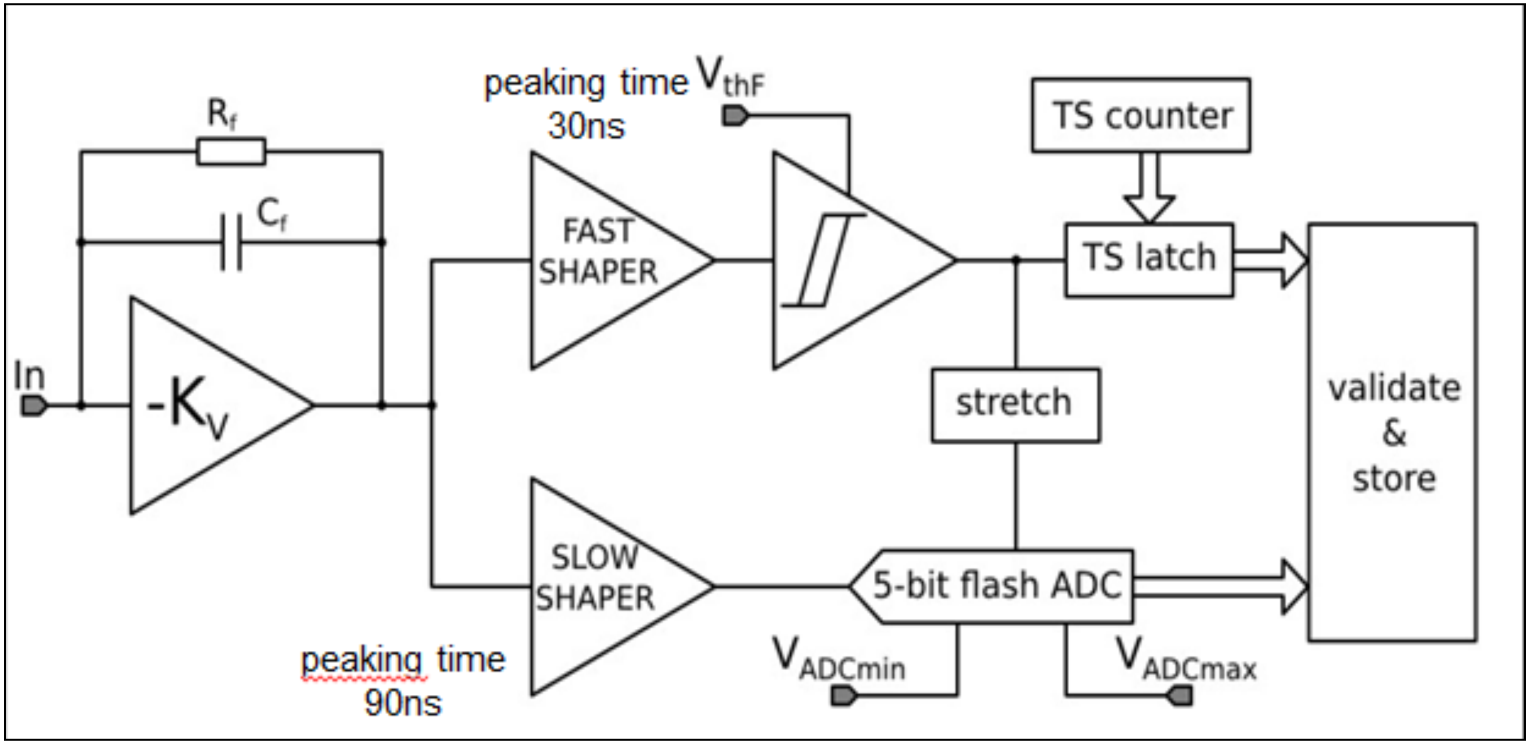

Particle finder

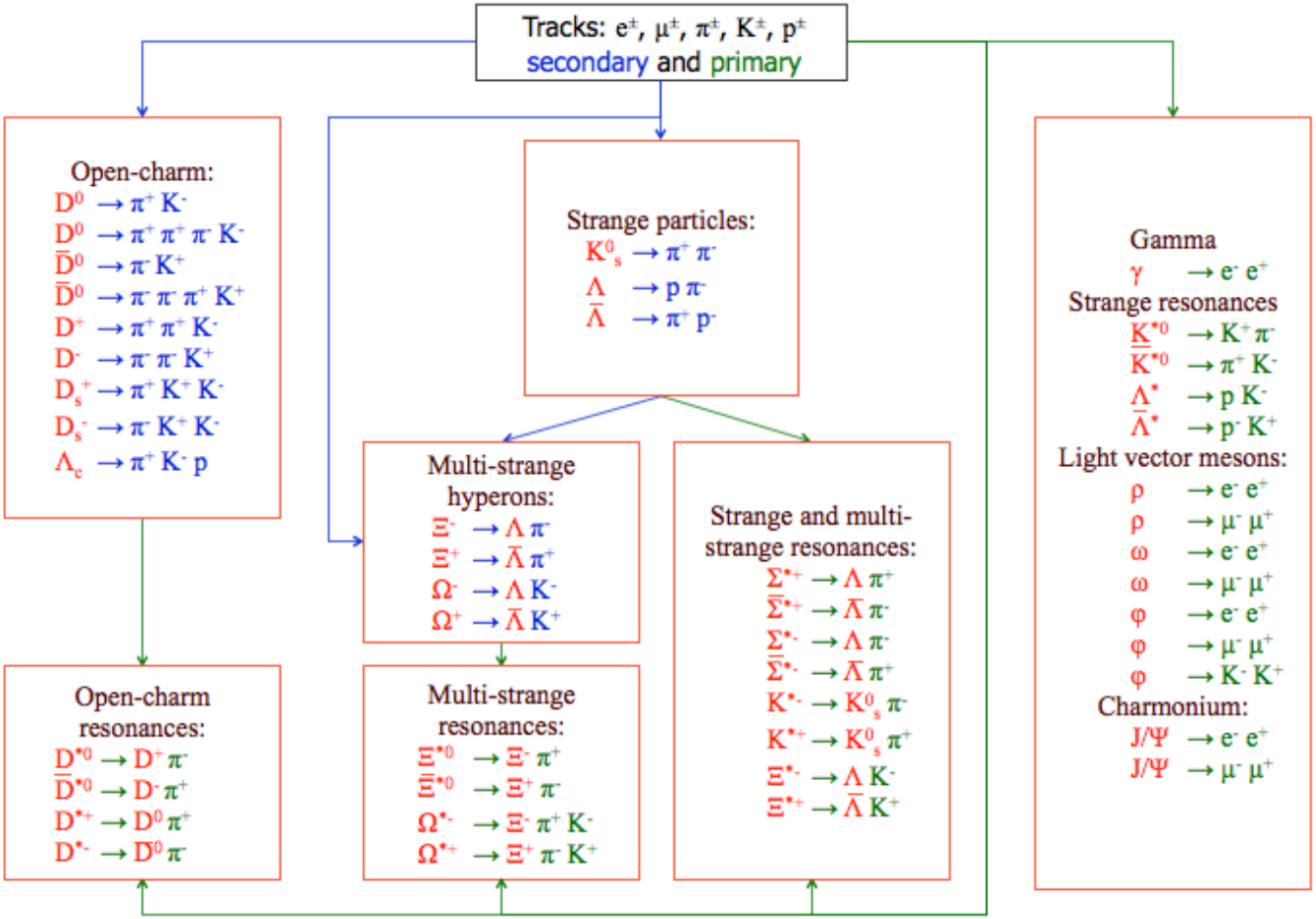

Tracks: $e^\pm$, $\mu^\pm$, $\pi^\pm$, $K^\pm$, $p^\pm$
secondary and primary

Open-charm:
$D^0 \rightarrow \pi^+ K^-$
$D^0 \rightarrow \pi^+ \pi^+ \pi^- K^-$
$\bar{D}^0 \rightarrow \pi^- K^+$
$\bar{D}^0 \rightarrow \pi^- \pi^- \pi^+ K^+$
$D^+ \rightarrow \pi^+ \pi^+ K^-$
$D^- \rightarrow \pi^- \pi^- K^+$
$D_s^+ \rightarrow \pi^+ K^+ K^-$
$D_s^- \rightarrow \pi^- K^+ K^-$
$\Lambda_c \rightarrow \pi^+ K^- p$

Strange particles:
$K^0_s \rightarrow \pi^+ \pi^-$
$\Lambda \rightarrow p \pi^-$
$\bar{\Lambda} \rightarrow \pi^+ p^-$

Multi-strange hyperons:
$\Xi^- \rightarrow \Lambda \pi^-$
$\Xi^+ \rightarrow \bar{\Lambda} \pi^+$
$\Omega^- \rightarrow \Lambda K^-$
$\Omega^+ \rightarrow \bar{\Lambda} K^+$

Strange and multi-strange resonances:
$\Sigma^{*+} \rightarrow \Lambda \pi^+$
$\bar{\Sigma}^{*+} \rightarrow \bar{\Lambda} \pi^-$
$\Sigma^{*-} \rightarrow \Lambda \pi^-$
$\bar{\Sigma}^{*-} \rightarrow \bar{\Lambda} \pi^+$
$K^{*-} \rightarrow K^0_s \pi^-$
$K^{*+} \rightarrow K^0_s \pi^+$
$\Xi^{*-} \rightarrow \Lambda K^-$
$\Xi^{*+} \rightarrow \bar{\Lambda} K^+$

Gamma
$\gamma \rightarrow e^- e^+$
Strange resonances
$K^{*0} \rightarrow K^+ \pi^-$
$\bar{K}^{*0} \rightarrow \pi^+ K^-$
$\Lambda^* \rightarrow p K^-$
$\bar{\Lambda}^* \rightarrow p^- K^+$
Light vector mesons:
$\rho \rightarrow e^- e^+$
$\rho \rightarrow \mu^- \mu^+$
$\omega \rightarrow e^- e^+$
$\omega \rightarrow \mu^- \mu^+$
$\varphi \rightarrow e^- e^+$
$\varphi \rightarrow \mu^- \mu^+$
$\varphi \rightarrow K^- K^+$
Charmonium:
$J/\Psi \rightarrow e^- e^+$
$J/\Psi \rightarrow \mu^- \mu^+$

Open-charm resonances:
$D^{*0} \rightarrow D^+ \pi^-$
$\bar{D}^{*0} \rightarrow D^- \pi^+$
$D^{*+} \rightarrow D^0 \pi^+$
$D^{*-} \rightarrow \bar{D}^0 \pi^-$

Multi-strange resonances:
$\Xi^{*0} \rightarrow \Xi^- \pi^+$
$\bar{\Xi}^{*0} \rightarrow \Xi^+ \pi^-$
$\Omega^{*-} \rightarrow \Xi^- \pi^+ K^-$
$\Omega^{*+} \rightarrow \Xi^+ \pi^- K^+$

Performance of hyperon and open charm measurements

$5 \cdot 10^6$ central Au+Au collisions, 10 AGeV

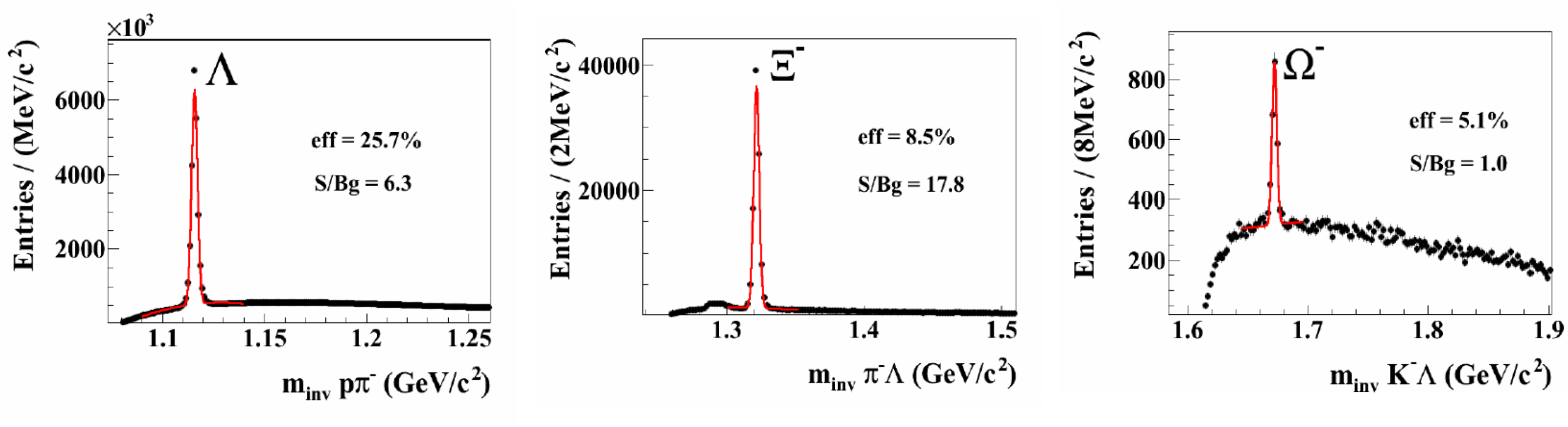

p+C collisions, 30 GeV (SIS100); 10^{12} centr.

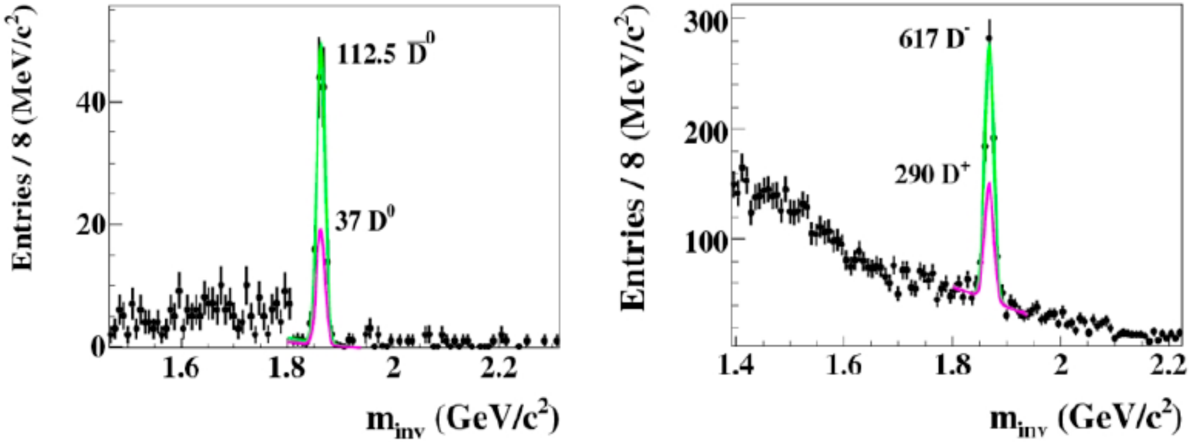

Micro Vertex Detector (MVD)

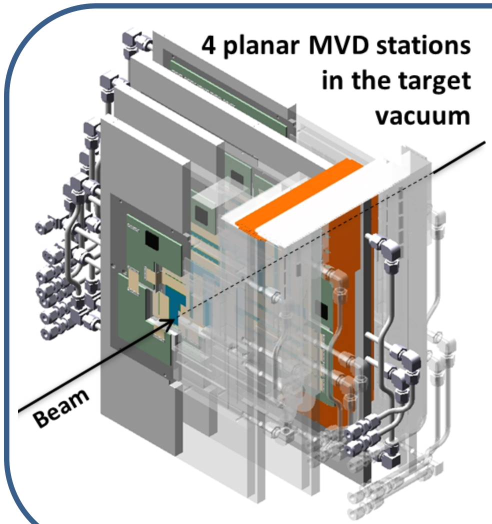

Ultra-thin: CVD diamond, TPG

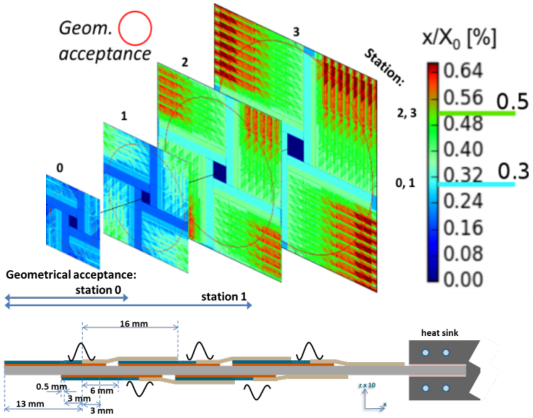

Sensors: CMOS MAPS

- *Radiation hard,*
- *Thinned to 50 µm,*
- *< 150 mW/cm^2,*
- *spatial resol. < 5 µm,*
- *R/O several 10 µs/frame*

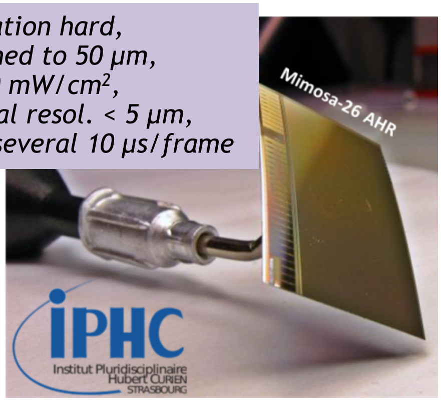

Prototyping & test

MVD demonstrator

MVD prototype

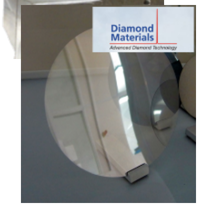

PRESTO

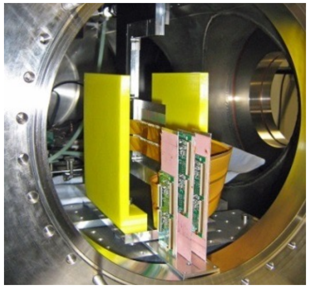

MOMENTIVE

Thermal Pyrolytic Graphite

Customized FEE & DAQ: TRB-based

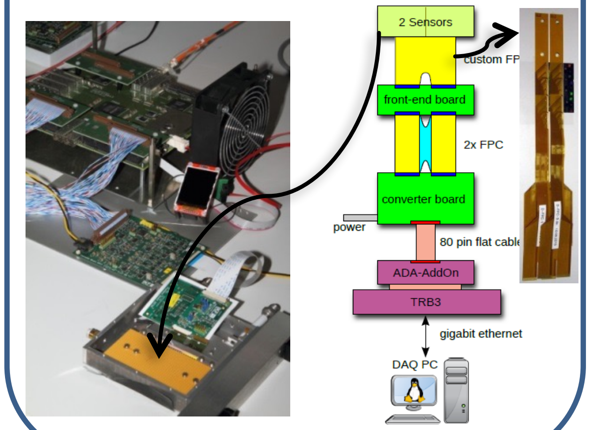

Energy loss: NIEL

NIEL:

- displacement damage;
- Frenkel pairs are produced;
- minimum E_d ~ 20 eV to produce a primary knock-on atom;
- charged particles: Rutherford scattering;
- neutral: mainly elastic scattering, but also nuclear reactions, e.g., $^{30}Si + n \rightarrow ^{31}Si + \gamma;\ ^{31}Si \rightarrow P + e^- + \overline{\nu}$

Maximum recoil energy that can be transferred (elastic scattering):

$$E_{R,max} = 4E_P \frac{m_P\, m_{Si}}{(m_P + m_{Si})^2}$$

1 MeV neutron: average $E_R \approx 50$ keV

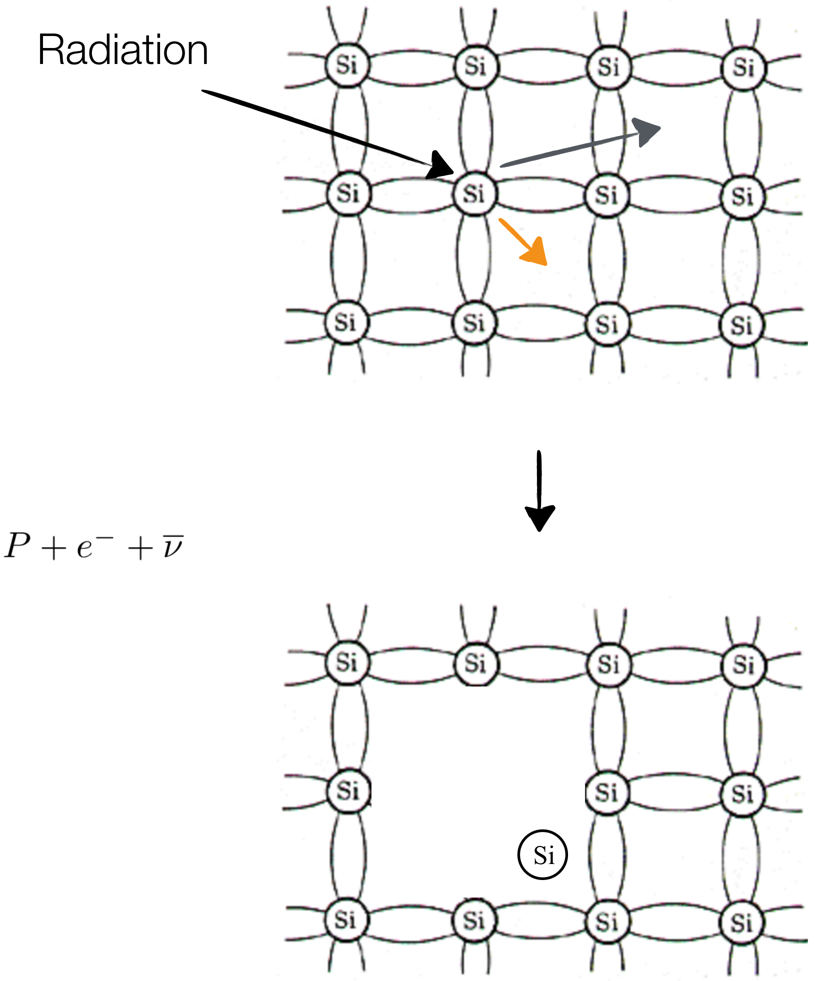

vacancy (V) + interstitial (I) pair

Energy loss: NIEL

Produced defects:

- recombine if located within the lattice cell; ≈ 60% of overall cases;
- are mobile at T > 100K, thus diffuse away - interact with other defects or bulk impurities (C, P, O, …);
- if $E_R > E_d$, produce further V-I pairs.

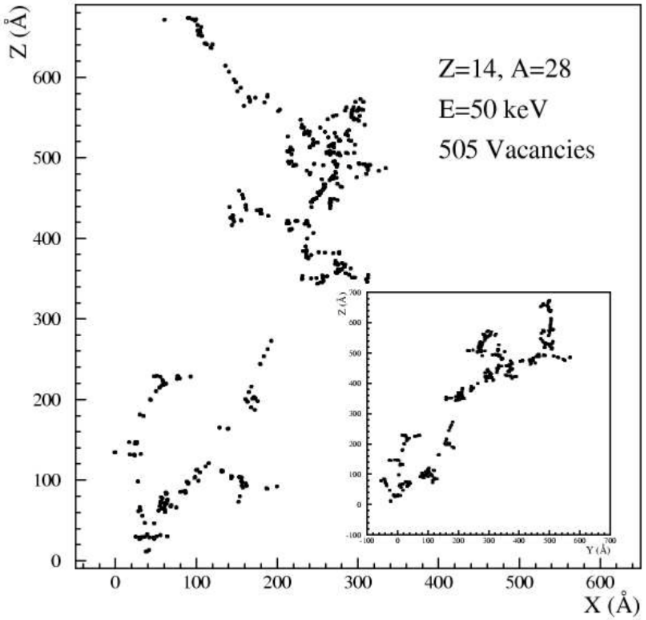

Simulated event of the 50 keV PKA:

~ 1000 vacancy-interstitial pairs;

plot by M. Huhtinen.

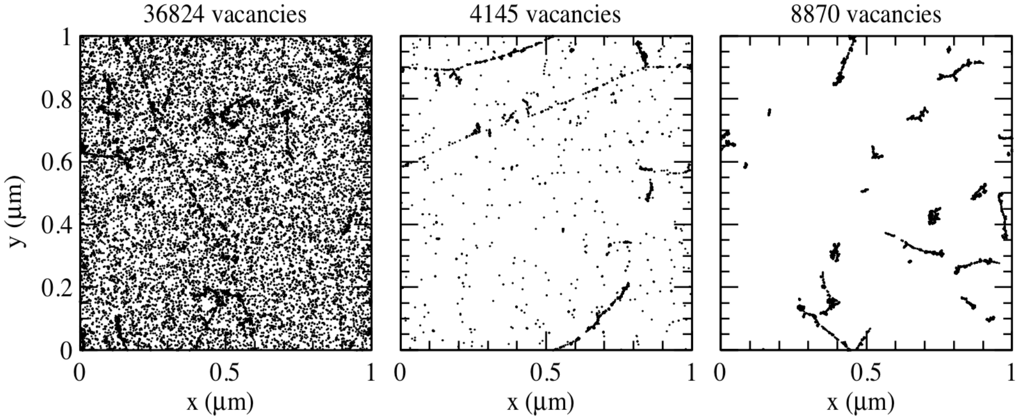

Simulation: initial distributions of vacancies by 10 MeV protons (left), 25 GeV protons (middle), 1 MeV neutrons (right). Corresponding fluence: 10^{14} cm^{-2}.

by M. Huhtinen.

NIEL scaling

The NIEL scaling hypothesis:

» the change in the material properties scales with the imparted energy;

» independent on the spacial distributions of the defects in one PKA cascade;

» independent on annealing sequences after the initial damage event.

Displacement damage function:

$$D(E) = \sum_i \sigma_i(E) \cdot \int_0^{E_{R,max}} f_i(E, E_R) P(E_R) dE_R$$

Hardness factor:

$$\kappa = \frac{\int D(E)\Phi(E)dE}{D(E_{n(1\ MeV)}) \cdot \int \Phi(E)dE}$$

Equivalent fluence:

$$\Phi_{eq}(1\ \mathrm{MeV\ neutrons}) = \kappa \cdot \Phi$$

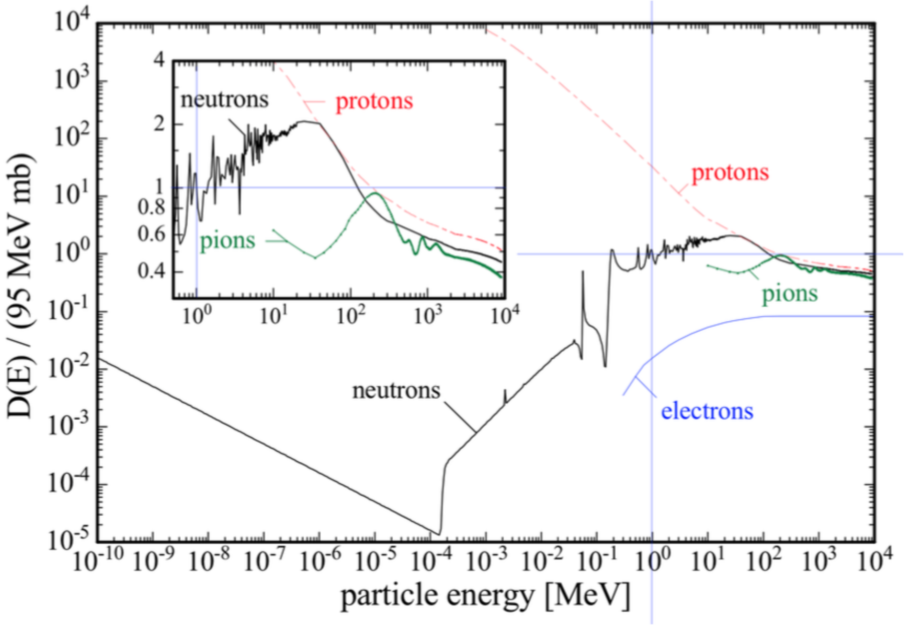

Displacement damage functions normalized to 95 MeV·mb for different particles. pic: G. Lindström.

Classification of defects

Defects:

- DLTS technique is used for characterisation of defects;
- Point defects: V, C, …;
- Complexes: > 1 constituents;
- Energy states: various;
- Charged states: various;
- Deep levels: E_t close to mid-gap.

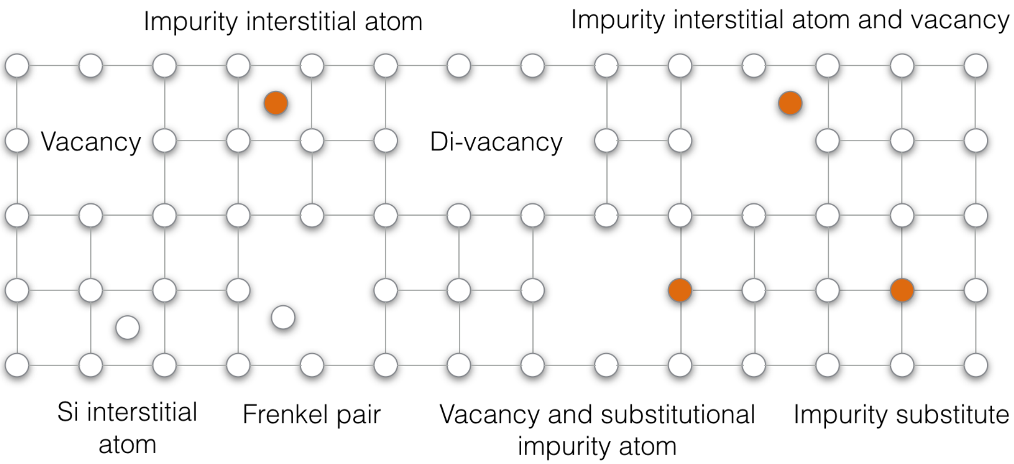

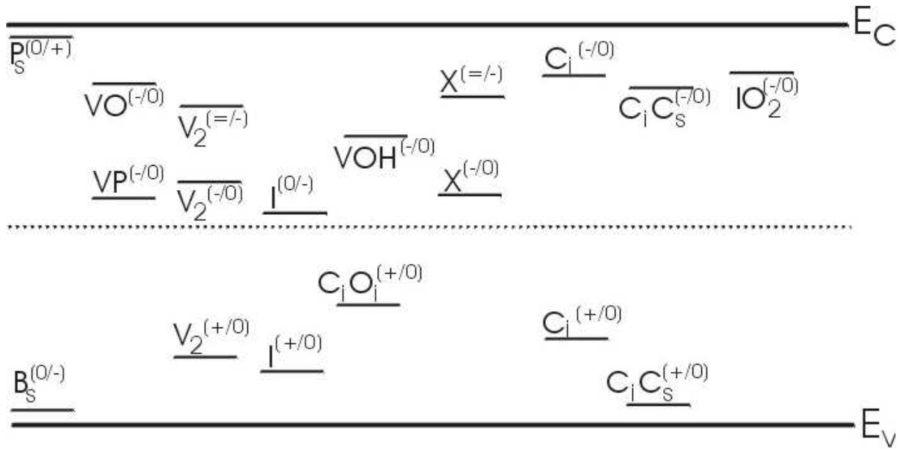

Pic: D. Contrato.

Consequences on detector operation

The deep level states:

- » Energy close to mid-gap: generate additional leakage current;
- » Charged → change the space charge density N_{eff} → change the V_{fd};
- » Trap carriers → reduce the charge collection; $1/\tau_{\mathrm{eff}}$ increases with fluence (more for holes than for electrons);
- » Time evolution (annealing): N_{eff}, I_{leak}, $1/\tau_{\mathrm{eff}}$ change.

Leakage current as a function of the fluence

Leakage current increases proportionally to the fluence:

$$\frac{\Delta I}{Volume} = \alpha \cdot \Phi_{eq}$$

$$(I \sim G \sim N_{DL} \sim \Phi_{eq})$$

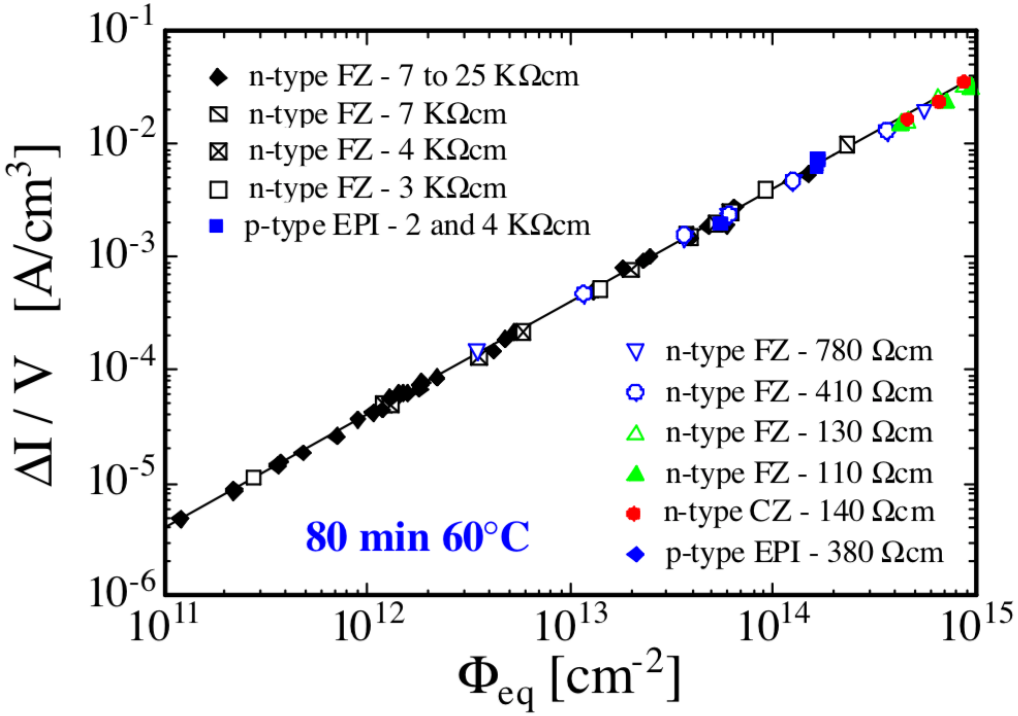

Leakage current density as a function of the accumulated fluence. Pic: G. Lindström.

α is the current damage rate:

- temperature dependent (usually given at 20 °C);
- $\alpha \approx 5\text{-}6 \times 10^{17}$ A/cm measured after irradiation.

Full depletion voltage as a function of the fluence

Full depletion voltage ~ effective doping concentration:

$$V_{fd} = \frac{d^2 q \mid N_{eff} \mid}{2\varepsilon\varepsilon_0}$$

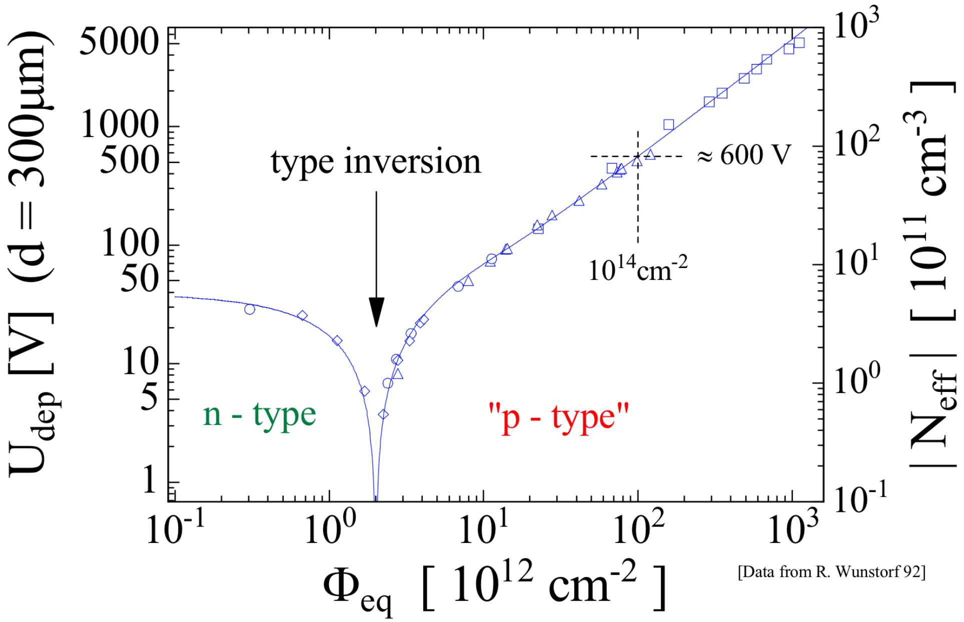

[Data from R. Wunstorf 92]

for the *n*-type silicon detector:

- » decrease of $|N_{eff}|$ → removal of donors (e.g., $V+P \rightarrow VP^{(-/0)}$), introduction of acceptor-like states;
- » space charge sign inversion;
- » linear increase of $|N_{eff}|$ with fluence after the SCSI;
- » evolution depends on $N_{eff,0} \rightarrow V_{fd,0}$;
- » preferable: as low as possible V_{fd} after irradiation beyond the SCSI.

Hamburg model

Change in effective impurity concentration can be parametrized:

$$\Delta N_{eff}(\Phi_{eq}, t) = N_C(\Phi_{eq}, t) + N_A(\Phi_{eq}, t) + N_Y(\Phi_{eq}, t),$$

N_C - stable damage;
N_A - short-term annealing;
N_Y - long-term annealing.

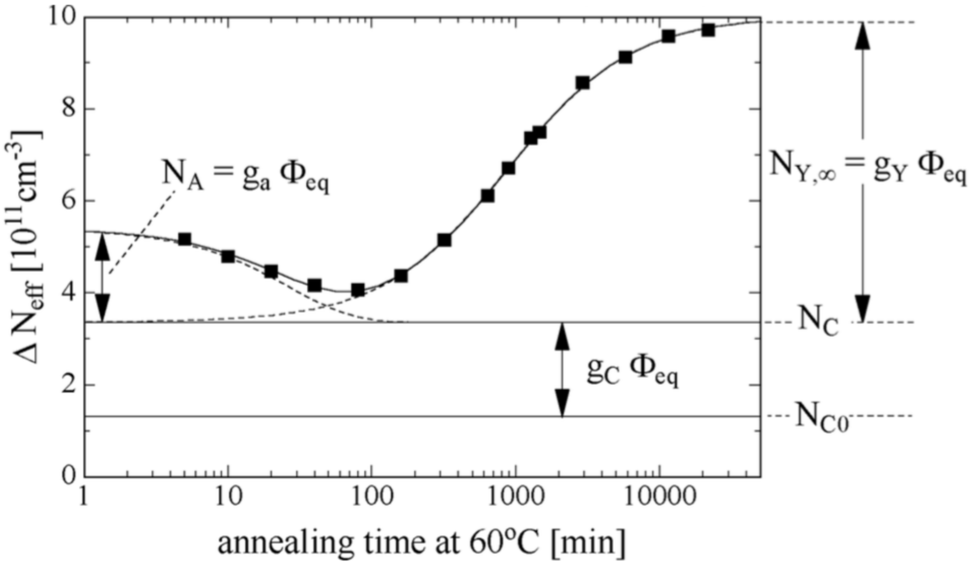

Picture: M. Moll.

Stable damage is described as:

$$N_C = N_{C0}\left(1 - \exp\left(-c\Phi_{eq}\right)\right) + g_c\Phi_{eq},$$

where c is the rate of donor removal, g_c is introduction of stable acceptors, $N_{C0} \approx 0.8 \times N_{eff,0}$.

Hamburg model

Change in effective impurity concentration can be parametrized:

$$\Delta N_{eff}(\Phi_{eq}, t) = N_C(\Phi_{eq}, t) + N_A(\Phi_{eq}, t) + N_Y(\Phi_{eq}, t),$$

N_C - stable damage;

N_A - short-term annealing;

N_Y - long-term annealing.

Stable damage is described as:

$$N_C = N_{C0}\left(1 - \exp\left(-c\Phi_{eq}\right)\right) + g_c\Phi_{eq},$$

where c is the rate of donor removal, g_c is introduction of stable acceptors, $N_{C0} \approx 0.8 \times N_{eff,0}$.

Calculation using the Hamburg model (N_C+N_A(t_a=0)), 290 μm sensor with various $N_{eff,0}$:

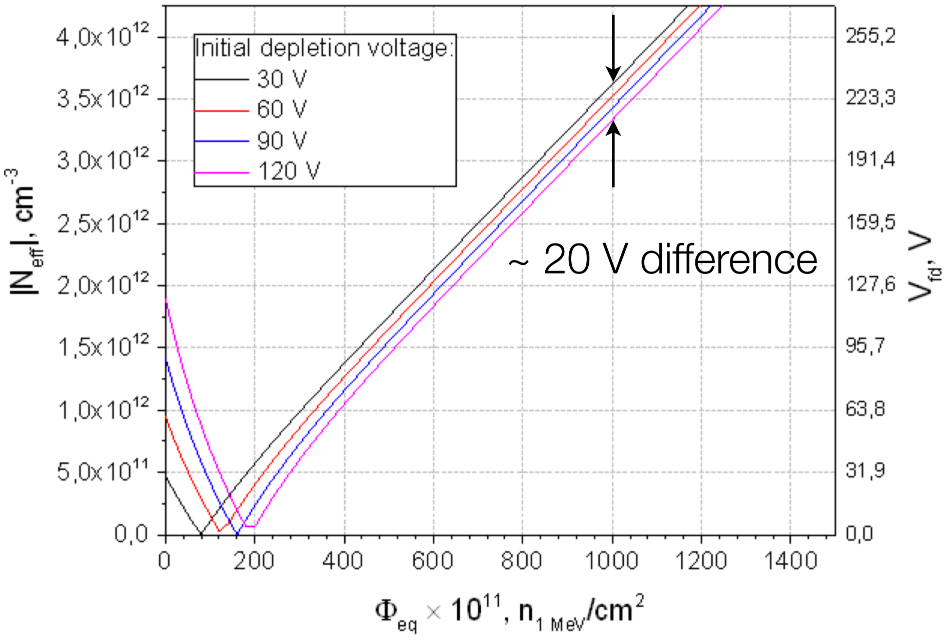

↓

c = 8.16×10^{14} cm^2

g_c = 1.9×10^{-2} cm^{-1}

Reduction of charge collection efficiency

Why? trapping of carriers:

- » trapped carriers do not move → no current is induced → signal reduced;
- » Main hole trap: $E_t = E_v + 0.34$ eV, electron: $E_t = E_c - 0.48$ eV [G. Kramberger];
- » Effective trapping time/probability is different for electrons and for holes [Transient Current Technique];
- » Carrier lifetime drops down to nanosecond level after heavy irradiation;
- » CCE:

$$Q_{e,h}(t) = Q_{0_{e,h}} exp\left(-\frac{1}{\tau_{eff_{e,h}}} \cdot t\right), \quad \text{where } \frac{1}{\tau_{eff_{e,h}}} \propto N_{defects}$$

$$\frac{1}{\tau_{\mathrm{eff}_{\mathrm{e,h}}}} = \Phi_{\mathrm{eq}} \sum_k g_k (1 - P_k^{\mathrm{e,h}}) \sigma_{k_{\mathrm{e,h}}} v_{\mathrm{th}_{\mathrm{e,h}}} = \beta_{\mathrm{e,h}}(t, T) \Phi_{\mathrm{eq}}$$

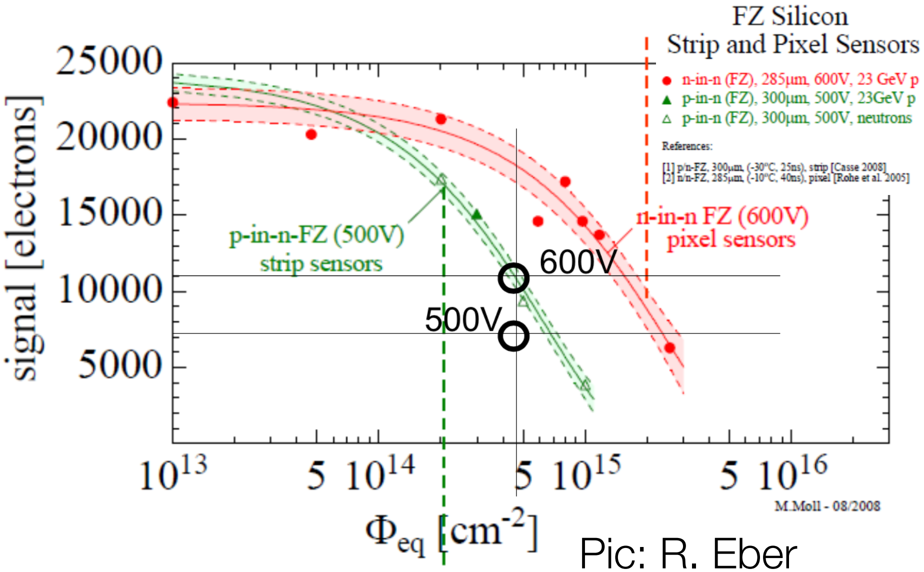

Pic: R. Eber

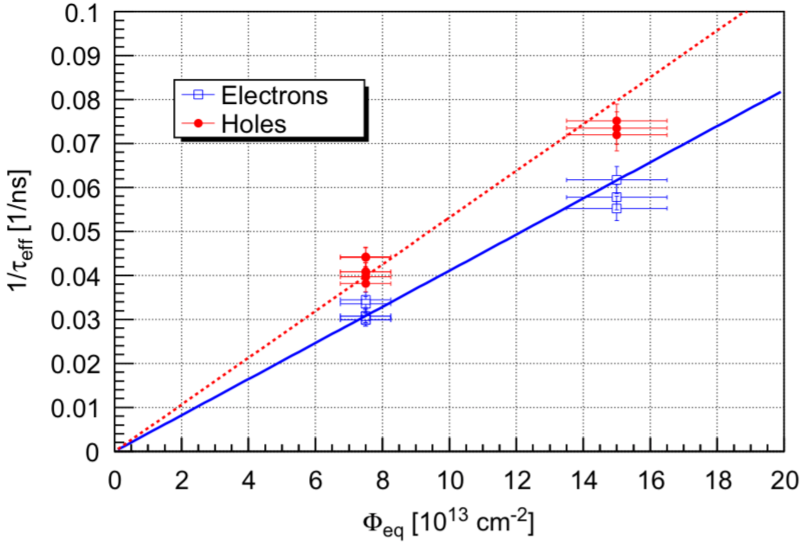

Pic: G. Kramberger

Time evolution of defects (annealing)

At finite temperatures the defects:

- Migrate and create complexes:
  $V+V = V_2$, $C_i + C_s \rightarrow C_iC_s$;
- Dissociate, e.g.,
  C_iC_s (≈ 250 ºC)$\rightarrow C_i + C_s$;
- So, annealing takes place already during irradiation.

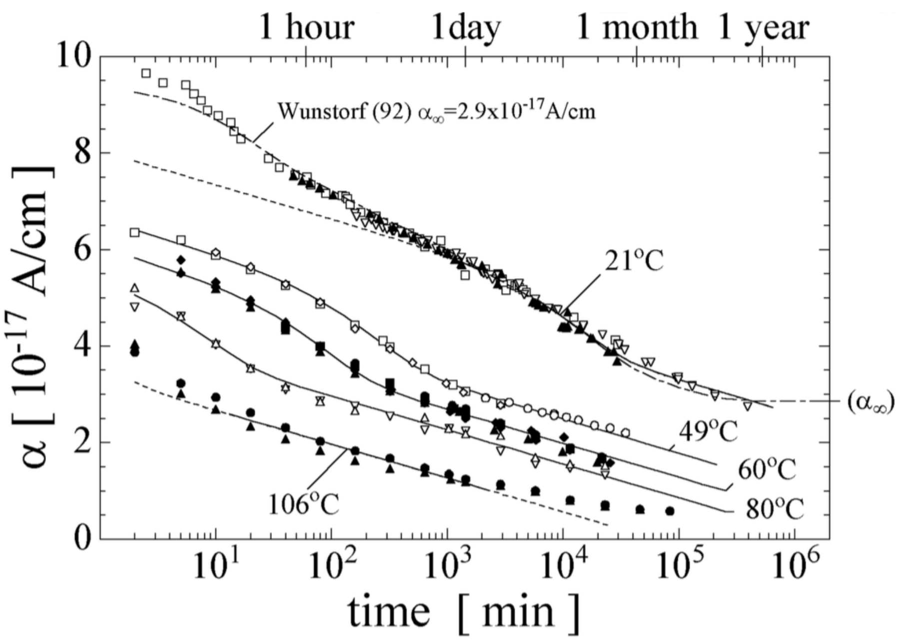

Picture: M. Moll.

Reverse current decreases as a function of time:

- $$\alpha(t) = \alpha_I \cdot exp\left(-\frac{t}{\tau_I}\right) + \alpha_0 - \beta \cdot ln\left(t/t_0\right)$$ [M. Moll]
- lower leakage current → lower the shot noise.

Time evolution of defects (annealing)

At finite temperatures the defects:

- Migrate and create complexes: *$V+V = V_2$, $C_i + C_s \rightarrow C_iC_s$;*
- Dissociate, e.g., *C_iC_s (≈ 250 ºC)$\rightarrow C_i + C_s$;*
- So, annealing takes place already during irradiation.

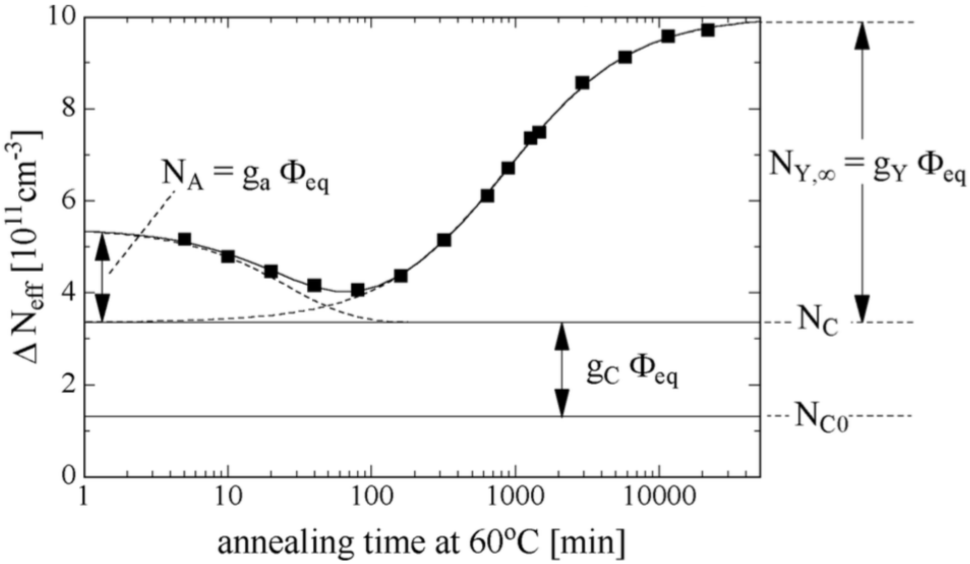

Picture: M. Moll.

Change in effective impurity concentration:

$$\Delta N_{eff}(\Phi_{eq}, t) = N_C(\Phi_{eq}, t) + N_A(\Phi_{eq}, t) + N_Y(\Phi_{eq}, t)$$

$$N_A = \Phi_{eq} \sum_i g_{a,i} \exp\left(-\frac{t}{\tau_{a,i}}\right)$$

g_a - average introduction rate, = 1.81±0.14×10^{-2} cm^{-1}

$$N_Y\left(t\right) = N_{Y,\infty}\left(1 - \frac{1}{1+t/\tau_Y}\right)$$

g_Y - average introduction rate, = 5.16±0.09×10^{-2} cm^{-1}

$N_{Y,\infty} = g_Y \cdot \Phi_{eq}$

Time evolution of defects (annealing)

At finite temperatures the defects:

- Migrate and create complexes: $V + V = V_2$, $C_i + C_s \rightarrow C_iC_s$;
- Dissociate, e.g., C_iC_s (≈ 250 ºC)→ $C_i + C_s$;
- So, annealing takes place already during irradiation.

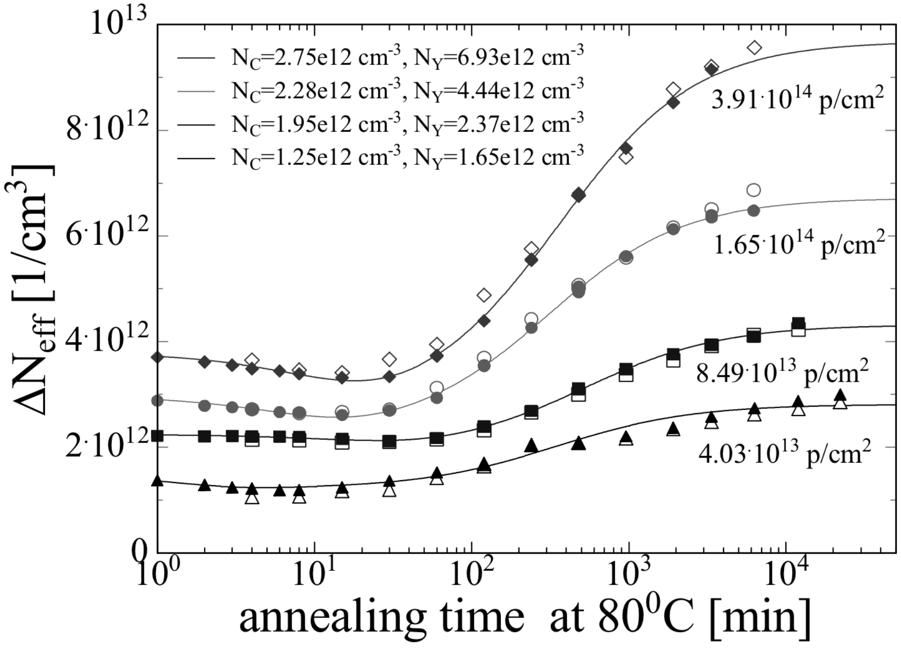

Picture: G. Lindström.

Change in effective impurity concentration:

$$\Delta N_{eff}(\Phi_{eq}, t) = N_C(\Phi_{eq}, t) + N_A(\Phi_{eq}, t) + N_Y(\Phi_{eq}, t)$$

$$N_A = \Phi_{eq} \sum_i g_{a,i} \exp\left(-\frac{t}{\tau_{a,i}}\right)$$

g_a - average introduction rate, = 1.81±0.14×10^{-2} cm^{-1}

$$N_Y(t) = N_{Y,\infty}\left(1 - \frac{1}{1 + t/\tau_Y}\right)$$

g_Y - average introduction rate, = 5.16±0.09×10^{-2} cm^{-1}

$N_{Y,\infty} = g_Y \cdot \Phi_{eq}$

Time evolution of defects (annealing)

At finite temperatures the defects:

- » Migrate and create complexes: $V+V = V_2$, $C_i + C_s \rightarrow C_iC_s$;
- » Dissociate, e.g., C_iC_s (≈ 250 ºC) $\rightarrow C_i + C_s$;
- » So, annealing takes place already during irradiation.

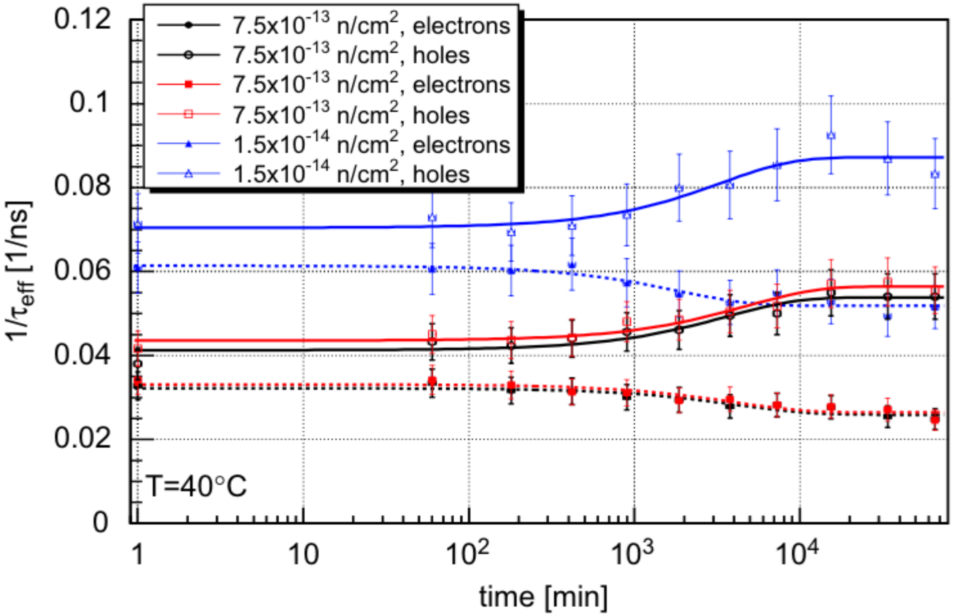

Picture: G. Kramberger *et.al*.

Change in effective trapping probability:

increases for holes, decreases for electrons → holes (collected at the *p*-side opposite to the junction after the SCSI) have shorter drift length.